Biochimica et Biophysica Acta 1803 (2010) 452–467

Contents lists available at ScienceDirect

Biochimica et Biophysica Acta

journal homepage: www.elsevier.com/locate/bbamcr

Statin-triggered cell death in primary human lung mesenchymal cells involves p53-PUMA and release of Smac and Omi but not cytochrome *c*

Saeid Ghavami [a,b,c], Mark M. Mutawe [a,c], Kristin Hauff [d], Gerald L. Stelmack [a,c], Dedmer Schaafsma [a,c], Pawan Sharma [a,b,c], Karol D. McNeill [a,c], Tyler S. Hynes [a,b,c], Sam K. Kung [e], Helmut Unruh [f], Thomas Klonisch [g], Grant M. Hatch [d], Marek Los [h], Andrew J. Halayko [a,b,c,f,*]

[a] *Department of Physiology, University of Manitoba, Winnipeg, MB, Canada*
[b] *National Training Program in Allergy and Asthma, University of Manitoba, Winnipeg, MB, Canada*
[c] *Biology of Breathing Group, Manitoba Institute of Child Health, Winnipeg, MB, Canada*
[d] *Department of Pharmacology, University of Manitoba, Winnipeg, MB, Canada*
[e] *Department of Immunology, University of Manitoba, Winnipeg, MB, Canada*
[f] *Department of Internal Medicine, University of Manitoba, Winnipeg, MB, Canada*
[g] *Department of Human Anatomy and Cell Science, University of Manitoba, Winnipeg, MB, Canada*
[h] *Interfaculty Institute of Biochemistry, Univ. Tuebingen, Germany*

ARTICLE INFO

Article history:
Received 5 October 2009
Received in revised form 16 December 2009
Accepted 16 December 2009
Available online 4 January 2010

Keywords:
Apoptosis
Statin
Caspase
Airway smooth muscle
Fibroblast
Mitochondria

ABSTRACT

Statins inhibit 3-hydroxy-3-methyl-glutarylcoenzyme CoA (HMG-CoA) reductase, the proximal enzyme for cholesterol biosynthesis. They exhibit pleiotropic effects and are linked to health benefits for diseases including cancer and lung disease. Understanding their mechanism of action could point to new therapies, thus we investigated the response of primary cultured human airway mesenchymal cells, which play an effector role in asthma and chronic obstructive lung disease (COPD), to simvastatin exposure. Simvastatin induced apoptosis involving caspase-9, -3 and -7, but not caspase-8 in airway smooth muscle cells and fibroblasts. HMG-CoA inhibition did not alter cellular cholesterol content but did abrogate *de novo* cholesterol synthesis. Pro-apoptotic effects were prevented by exogenous mevalonate, geranylgeranyl pyrophosphate and farnesyl pyrophosphate, downstream products of HMG-CoA. Simvastatin increased expression of Bax, oligomerization of Bax and Bak, and expression of BH3-only p53-dependent genes, PUMA and NOXA. Inhibition of p53 and silencing of p53 unregulated modulator of apoptosis (PUMA) expression partly counteracted simvastatin-induced cell death, suggesting a role for p53-independent mechanisms. Simvastatin did not induce mitochondrial release of cytochrome *c*, but did promote release of inhibitor of apoptosis (IAP) proteins, Smac and Omi. Simvastatin also inhibited mitochondrial fission with the loss of mitochondrial Drp1, an essential component of mitochondrial fission machinery. Thus, simvastatin activates novel apoptosis pathways in lung mesenchymal cells involving p53, IAP inhibitor release, and disruption of mitochondrial fission.

1. Introduction

Due to structural similarity with 3-hydroxy-3-methyl-glutaryl-CoA (HMG-CoA), statins such as simvastatin, lovastatin and atorvastatin, inhibit HMG-CoA reductase, the proximal rate-limiting enzyme in cholesterol biosynthesis [1]. They effectively lower serum cholesterol but overall benefits exceed that predicted by this outcome alone, suggesting additional cholesterol-independent effects [2]. Thus, the impact of statins on disease states including cancer, neurological disorders, diabetes, kidney disease, lung infection, and chronic inflammatory lung disease, is being assessed in clinical trials [2,3]. HMG-CoA reductase catalyzes the conversion of HMG-CoA to the fatty acid mevalonate [2], which undergoes stepwise conversion into isoprenoids, farnesyl pyrophosphate (FPP) and geranylgeranyl pyrophosphate (GGPP). Isoprenoids can be covalently linked to signaling

Abbreviations: AIF, apoptosis-inducing factor; DISC, death-induced signaling complex; Drp1, dynamin-related protein 1; Endo G, Endo nuclease G; FADD, Fas-Associated Death Domain; FPP, farnesyl pyrophosphate; GGPP, geranylgeranyl pyrophosphate; GAPDH, Glyceraldehyde 3-phosphate dehydrogenase; HASM, Human airway smooth muscle; HAF, Human airway fibroblast; HMG-CoA, 3-hydroxy-3-methyl-glutaryl-CoA; HtrA2, high-temperature requirement A2; IAP, inhibitor of apoptosis protein; IBM, IAP binding motif; JC-1, 5,5′,6,6′-tetrachloro-1,1′,3,3′-tetraethylbenzimidazolylcarbocyanine iodide; $\Delta\Psi_m$, mitochondrial trans-membrane potential; MTT, 3-(4,5-dimethyl-2-thiazolyl)-2,5-diphenyl-2H-tetrazolium bromide; NAC, N-acetyl-L-cysteine; PCD, programmed cell death; PUMA, p53 unregulated modulator of apoptosis; ROS, reactive oxygen species; shRNAi, small hairpin inhibitory RNA; Smac, second mitochondria-derived activator of caspases; XIAP, X-linked inhibitor of apoptosis protein

* Corresponding author. Departments of Physiology and Internal Medicine University of Manitoba, Winnipeg, MB, Canada. Tel.: +1 204 787 2062.
E-mail address: ahalayk@cc.umanitoba.ca (A.J. Halayko).

0167-4889/$ – see front matter © 2009 Elsevier B.V. All rights reserved.
doi:10.1016/j.bbamcr.2009.12.005

proteins, in particular to members of the Ras superfamily, enabling attachment to lipid membranes required for activation and subsequent regulation of critical cell functions [4]. Suppression of protein prenylation is a key component of the broad effects of statins, but is it unclear if there are other cholesterol-independent mechanisms that underpin functional effects in different cell types. Understanding these mechanisms offers potential to identify new therapies to prevent or reverse human disease.

Statins can induce apoptosis in some cancer cell lines, primary cultured vascular smooth muscle, mesangial cells, and fibroblasts [5–7]. Consistent with a role for FPP and GGPP in this response, isoprenoid replacement overcomes pro-apoptotic effects of statins, the selective inhibition of farnesyl- and geranylgeranyl transferases can mimic pro-apoptotic effects, and prenylation-dependent membrane-associated GTPase signaling pathways may mediate the response [5,8,9]. Nonetheless, more downstream apoptotic signaling induced by statins remains incompletely understood. Apoptosis is under complex control by a receptor-mediated extrinsic pathway, and an intrinsic pathway triggered by a wide range of cellular stressors [10]. The intrinsic pathway is chiefly regulated by Bcl-2 family proteins via the disruption of mitochondrial trans-membrane potential ($\Delta\Psi_m$) and the formation of membrane permeability pores through which mitochondrial proteins are released to promote activation of caspase-9 [11]. For example, pro-apoptotic Bax and Bak proteins associate and form mitochondrial permeability pores, a process that can be inhibited by anti-apoptotic proteins such as Bcl-xL [12]. Pro-apoptotic proteins also include BH3-only proteins, such as p53-upregulated modulator of apoptosis (PUMA) and NOXA [10,13], which can inhibit the anti-apoptotic action of Bcl-xL to promote p53 assisted mitochondrial membrane translocation of Bax and Bak [12,14]. Proteins released from mitochondria include cytochrome *c*, which together with caspase-9, (d)ATP, and Apaf-1 form apoptosomes. Like its extrinsic pathway counterpart caspase-8, caspase-9 cleaves and activates caspase-3 and -7 to drive the execution phase of apoptosis [15]. Mitochondria also release Smac/DIABLO and Omi/HtrA2 that bind to, and suppress inhibitor of apoptosis proteins (IAPs) that otherwise prevent caspase activity [16,17].

Almost all data on statin-induced apoptosis have been obtained on cancer cell lines and there remains some controversy. Statins induce chromatin condensation and DNA laddering [18,19], and in a few cases activate caspase-8 as well as an upstream receptor, FAS/CD95 [20]. Notably, in human T-, B-, and myeloma tumor cells statin exposure activates both caspase-8 and -9, disrupts $\Delta\Psi_{tm}$, and promotes release of Smac from mitochondria [20]. However, inhibition of caspase-8 has no effect on apoptosis induction by lovastatin in mammary carcinoma [18]. In contrast, inhibitors of caspase-9 or executioner-caspases suppress statin-induced apoptosis [18]. Lovastatin-induced apoptosis has been shown to depend on the loss of the anti-apoptotic protein Bcl-2 in acute mylogeneous leukemia cells. In p53-deficient cultured breast cancer cells statins can induce mitochondrial translocation of Bax with a concomitant loss of mitochondrial membrane potential ($\Delta\Psi_m$) [8,18]. Thus, so far published data do not clearly depict the downstream mechanisms involved in statin-triggered apoptosis in cancer cells. Furthermore, despite extensive medical use the potential, and mechanisms of apoptosis induction by statins in primary cells have not been systematically investigated.

In this study we investigated apoptosis mechanisms invoked by HMG-CoA reductase inhibition in human lung mesenchymal cells. We found that simvastatin induced apoptosis via a novel intrinsic pathway. Studies were performed on primary cultured human airway smooth muscle (HASM) cells and airway fibroblasts (HAF) as these cells underpin acute and chronic wound healing and inflammation associated with prevalent lung diseases such as asthma, chronic obstructive lung disease (COPD), and cystic fibrosis [21,22]. Indeed, there is new evidence suggesting statins have beneficial effects on these conditions [23–25]. Moreover, many therapies under development for these pathologies aim to reduce airway mesenchymal cell number. Thus, unraveling mechanisms of statin-mediated cell death within HAF and HASM may reveal new therapeutic targets.

2. Methods

2.1. Reagents

Cell culture plasticware was obtained from Corning Costar Co. (Canada). Cell culture media, propidium iodide (PI), simvastatin, NS3694, mevalonate, farnesyl pyrophosphate (FPP), geranylgeranyl pyrophosphate (GGPP), cyclic Pifithrin-α, and 3-(4,5-dimethyl-2-thiazolyl)-2,5-diphenyl-2H-tetrazolium bromide) (MTT), and N-acetyl-L-cysteine (NAC) were obtained from Sigma (Sigma-Aldrich, Oakville, CA). [14C]acetate and [14C]mevalonate were purchased from Perkin Elmer (Vaudreuil-Dorion, Quebec PQ). Rabbit anti-human cleaved caspase-6, -7, -8, poly ADP-ribose polymerase (PARP), rabbit anti-human Bak, Bax, PUMA, Bcl-2, Bid, phospho-p53 (Ser 15) and (Ser 37), Rac1/2/3, p21 and cytochrome *c* were purchased from Cell Signaling (Canada). Rabbit anti-Drp1, rabbit anti-glyceraldehyde-3-phosphate dehydrogenase (GAPDH), rabbit anti-Smac/DIABLO, rabbit anti-Omi/HtrA2, mouse anti-cytochrome *c*, and goat anti-endonuclease G (Endo G) were obtained from Santa Cruz Biotechnologies (USA). Mouse anti-p53 and anti-NOXA were obtained from Abcam (USA). 5,5′,6,6′-tetrachloro-1,1′,3,3′-tetraethylbenzimidazolylcarbocyanine iodide (JC-1), Mitotracker Red, and Mitosox were obtained from Invitrogen Molecular Probes (Canada). Caspase-Glo®-3/7, Caspase-Glo®-8 and Caspase-Glo®-9 assay were purchased from Promega (USA). N7-Smac peptide (cell permeable) was purchased from Calbiochem (Canada).

2.2. Primary HASM and HAF cell culture preparation

For all experiments we used primary cultured human airway smooth muscle (HASM) cells and airway fibroblasts (HAF) that were prepared from 2–4th generation bronchi in macroscopically healthy segments of resected lung specimens. After microdissection to separate the lamina reticularis and submucosal compartment from encircling airway smooth muscle bundle, HAF and HASM, respectively, were isolated by enzymatic dissociation as we have described [26,27]. All procedures were approved by the Human Research Ethics Board (University of Manitoba) and all donors gave informed consent. Unless otherwise stated cells were cultured in Dulbecco's modified Eagle's medium (DMEM) supplemented with 10% fetal bovine serum (FBS) and medium was changed every 48 h. For all experiments, *passage* 3–7 of HASM and HAF were used.

2.3. Cell viability-, cell death-, and related assays

Cytotoxicity of simvastatin towards the HASM and HAF was determined by MTT-assays as previously described [16]. Apoptosis was measured using the Nicoletti method as we have described previously [16]. Luminometric assays Caspase-Glo®-8, -9 and -3/7 (Promega, Canada, Nepean, ON) were used to measure the proteolytic activity of caspases-3/7 (DEVD-ase), -8 (IETD-ase), and -9 (LEHD-ase) as we have previously done [28]. Mitochondrial membrane potential was measured employing the mitochondria-specific cationic ratiometric dye JC-1 that undergoes $\Delta\Psi_m$-dependent aggregation in the mitochondria: JC-1 exists as a green fluorescent (540 nm, excitation 490 nm) monomer at $\Delta\Psi_m < 140$ mV, but when $\Delta\Psi_m > 140$ mV JC-1 aggregates and emit red fluorescence (590 nm, excitation 540 nm) [16,29].

2.4. Quantitative analysis of nuclear DNA fluorescence using laser scanning cytometry

Human bronchial smooth muscle cells were plated in 12 well cell culture clusters and grown to 80% confluence, maintained for 48 h in

DMEM/0.5% FBS, prior to addition of simvastatin (10 μM) or vehicle for 96 h. Fluorescent staining of live cell nuclear DNA was carried out by incubation in HBSS containing 5 μg/mL H33342 dye (15 min, 37 °C). Quantification of nuclear DNA fluorescence was carried out at room temperature using an iCYS laser scanning cytometer (Compucyte Corp., Westwood, MA, USA). Signals for blue channel fluorescence (Ex: 405 nm; Em: 463/39 nm) from contoured cell nuclei and light scatter data (488 nm argon laser line) for shaded relief images were captured. The DNA content data, collected from a circular scan area 0.12 cm^2 with individual scan field dimensions of 400×384 μm, included total integrated fluorescence and maximum pixel fluorescence, which provides a measure of nuclear condensation, within the boundary of each contoured cell nucleus. As photomultiplier (PMT) detectors have a bit depth of 14, individual pixel elements may have grey level values between 0–16,384.

2.5. Analysis of cellular morphology

To assess cell viability based on gross cellular appearance (chromatin condensation and cell shrinkage) HASM and HAF cells grown on 12 well plates were assessed by phase contrast microscopy (Olympus CK40) using a Olympus DP10 CCD digital camera to capture images.

2.6. Total cellular cholesterol assay

HASM and HAF cells (48 h in 0.5% FBS) were treated with simvastatin (10 μM) of vehicle (DMSO) for 48 or 96 h, then cells were harvested, washed with cold PBS, and centrifuged (800×*g*, 5 min). Cells were mixed with a 1:1 water–methanol solution and then a 1:5 water–chloroform solution before centrifuged in desktop microfuge (800×*g*, 10 min). The organic phase was dried and then isopropyl alcohol and Triton X-100 (0.1%) was added to cells to extract cholesterol, which was subsequently quantified using the Amex Invitrogen Cholesterol Assay according to the manufacturer's protocol. The assay uses enzyme-coupled reactions that hydrolyzed cholesteryl esters by cholesterol esterase into cholesterol, and then all cholesterol into H_2O_2 and a ketone by cholesterol oxidase. H_2O_2 is detected using 10-acetyl-3,7-dihydroxyphenoxazine, which in the presence of horseradish peroxidase (HRP) emits fluorescence in 1:1 stoichiometry with H_2O_2 [30,31].

2.7. Cholesterol de novo synthesis assay

HASM and HAF cells (48 h, 0.5% FBS) were treated with simvastatin (10 μM) or vehicle control (DMSO) for up to 96 h and cholesterol synthesis was determined using a modification of the Mokashi protocol [32]. [^{14}C]Acetate (Perkin Elmer, 60 mCi/mmol) was added (1 μCi/well), cells were incubated at 37 °C overnight. Mevinolin (1 μM, Sigma Chemical) was included in incubations with [^{14}C]mevalonate to block HMG-CoA reductase, and lipid-replete serum was used in all studies. Medium was removed, cells washed twice with 1% PBS (pH 7.4), harvested by scraping, re-suspended in 20 mM Tris–EDTA (pH 7.4) containing 0.1% Triton X-100, and then lysed by sonication at medium setting three times for 5 s with a Sonic Dismembrator (Fisher Scientific, Canada). Lipids were extracted without saponification (to allow quantitation of cholesterol-esters) with a mixture of chloroform/methanol (2:1), subjected to centrifugal evaporation, re-suspended in 50 μL of same and then resolved by silica thin-layer chromatography (Whatman) in petroleum ether/ethyl ether/acetic acid (60:40:1). Radiolabeled cholesterol and cholesterol-esters were visualized and quantified by electronic autoradiography (Packard Instant Imager) and authenticated by comparison to standards visualized by iodine-vapor stain. Cholesterol was also authenticated by gas-chromatographic/mass spectrometry of eluted samples.

2.8. Membrane anchoring of Rho GTPases

For determination of membrane anchoring of prenylated Rho and Rac GTPases, HASM cells were cultured in DMEM/0.5% FBS in the presence or absence of simvastatin (10 μM), and after washing cells were scraped in ice cold buffer (10 mM Tris–HCl, pH 7.5, 0.1 mM EDTA, 0.1 mM EGTA, 1 mM dithiothreitol, and protease inhibitor cocktail), sonicated on ice 3 times for 5 s, and then the homogenate was separated into cytoplasmic and membrane fractions by ultracentrifugation (100,000×*g* for 35 min) [33]. The membrane fractions were solubilized in dissociation buffer (50 mM Tris–HCl, pH 7.5, 0.15 M NaCl, 1 mM dithiothreitol, 1% SDS, 1 mM EDTA, 1 mM EGTA, protease inhibitor cocktail), and subsequently size fractioned by SDS-PAGE for immunoblot analysis using anti-Rac1/2/3 and anti-RhoA primary antibodies (Cell Signaling).

2.9. MitoSox reactive oxygen species assay

As mitochondria can be a source of ROS, we used cell permeant MitoSOX™ Red, which can be oxidized selectively by mitochondrial superoxide, a reaction is prevented by superoxide dismutase in live cells, but that is not subject to effects of other ROS^{-} or reactive nitrogen species (RNS). Once in the mitochondria, dye oxidized by superoxide exhibits red fluorescence. HASM and HAF sub-cultured in 12 well plate (35,000 cells/well) DMEM/0.5% FBS were treated with simvastatin (10 μM) or vehicle for up to 72 h, then 5 μM MitoSOX™ reagent was added for 10 min (37 °C) in the dark. After washing cell DNA was stained with Hoechst 33256 (5 μg/mL, 15 min), fixed (4% parafomaldehyde, 120 mM sucrose) and cell staining quantified using a iCys Laser Scanning Cytometry (LSC) (CompuCyte Corporation, Cambridge, MA).

2.10. Immunoblotting

We used Western blotting to detect cleaved caspase-8, -3, -9, -6, -7 PARP, Blc2, Bid, PUMA, NOXA, Bax, DRP1, hFIS1, p53, phosphor-p53 (Ser 15 and Ser37), Smac/DIABLO, Omi/HrA2, cytochrome *c*, Mn-SOD2, and GAPDH. Briefly, cells were washed and protein extracts prepared in lysis buffer (20 mM Tris–HCl (pH 7.5), 0.5% Nonidet P-40, 0.5 mM PMSF, 100 μM β-glycerol 3-phosphate and 0.5% protease inhibitor cocktail). After a high-speed spin (13,000*g*×10 min) supernatant protein content was determined by Lowry protein assay, then proteins were size fractionated by SDS-PAGE and transferred on to nylon membranes under reducing conditions, except for assessment of Bak dimerization, with proteins separated under non-reducing conditions. After blocking membranes with non-fat dried milk and Tween 20, blots were incubated overnight with the primary antibodies at 4 °C. HRP-conjugated secondary antibody incubation was for 1 h at room temperature, then blots were developed by enhanced chemiluminescence (ECL) detection (Amersham-Pharmacia Biotech). In experiments detecting Bak oligomerization non-reducing immunoblotting was used.

2.11. Immunocytochemistry, confocal imaging and electron microscopy

For immunocytochemistry, HASM and HAF cells were grown overnight on coverslips and then treated with simvastatin (10 μM) or vehicle for 72 h prior to fixation (4% paraformaldehyde/120 mM sucrose) and permeabilization (0.1% Triton X-100). Cells were incubated with rabbit anti-DIABLO IgG (1:150), goat anti-Endo G IgG (1:75), or mouse anti-AIF IgG (1:75), then with corresponding fluorochrome-conjugated secondary antibodies. Thereafter, mitochondria were stained with Mitotracker Red CMXRos (Molecular Probes; 200 nM). The fluorescent images were then observed and analyzed using an Olympus FluoView multi-laser confocal microscope. For transmission electron microscopy (TEM), cells were fixed

(2.5% glutaraldehyde in PBS (pH 7.4) for 1 h at 4 °C) and post-fixed (1% osmium tetroxide) before embedding in Epon. TEM was performed with a Philips CM10, at 80 kV, on ultra-thin sections (100 nm on 200 mesh grids) stained with uranyl acetate and counterstained with lead citrate.

2.12. Subcellular fractionation

Cytosolic and mitochondrial fractions were generated using a digitonin-based subcellular fractionation technique at 4 °C [34]. Cells were scraped, pelleted by centrifugation (800×*g*), then washed (PBS pH 7.2) and re-centrifuged. Pellets were permeabilized for 5 min on ice: 3×10^7 cells/mL of cytosolic extraction buffer (250 mM sucrose, 70 mM KCl, 137 mM NaCl, 4.3 mM Na2HPO4, 1.4 mM KH_2PO_4 pH 7.2, 100 μM PMSF, 10 μg/mL leupeptin, 2 μg/mL aprotinin, containing 200 μg/mL digitonin). Plasma membrane permeabilization was confirmed by staining with 0.2% trypan blue solution then cells were pelleted (1000×*g*, 5 min). The supernatant (cytosolic fractions) was removed, then pellets were solubilized in the same volume of mitochondrial lysis buffer (50 mM Tris pH 7.4, 150 mM NaCl, 2 mM EDTA, 2 mM EGTA, 0.2% Triton X-100, 0.3% NP-40, 100 μM PMSF, 10 μg/mL leupeptin, 2 μg/mL aprotinin), followed by pelleting at 10,000×*g* for 10 min at 4 °C. Supernatant was collected as mitochondrial fraction. For the detection of specific protein by immunoblotting proteins, an equal amount of cytosolic and pellet fraction protein were supplemented with 5×SDS-PAGE loading buffer, subjected to standard 12% or 15% SDS-PAGE and transferred to nitrocellulose membranes.

2.13. Stable gene silencing: lentiviral delivery of shRNA

All short hairpin (sh)RNA containing constructs were from Open Biosystems distributed by the Biomedical Functionality Resource, at University of Manitoba. The PUMA shRNA construct (accession # NM_014417, cat# RHS3979-9601020), distributed in a bacterial culture of *E. coli* (DH5α), included a "stem" of 21 sense (GAGGGTCCTG-TACAATCTCAT) and antisense base pairs and a 6 base pair loop, cloned into the lentiviral vector pLKO1. Individual colonies were grown up in LB broth with ampicillin (100 μg/mL), purified using a Qiagen Maxi-prep Kit (cat# 12663, Mississauga, ON). A vesicular stomatitis virus G (VSVG) pseudo-typed lentiviral vector was made using HEK 293T cells by calcium phosphate transfection of purified PUMA shRNA plasmid, virus packaging vector (8.2Δvpr), and a VSVG plasmid as described previously [35]. After 3 days the supernatant was collected and concentrated by ultra-centrifugation (17,000 rpm for 90 min). Primary HASM cells were grown to 70% confluence and transduced at a MOI of 6, in the presence of 8 μg/mL polybrene (final concentration), for 2 h. Excess viral vectors were removed, and the transduced cells were cultured in fresh medium for 2 days before puromycin selection. Cells exhibiting stable expression of the shRNA were selected by growing in culture media containing puromycin (4 μg/mL) for at least 3 weeks. For control cells, in tandem with preparation of PUMA shRNAi lentivirus a pLKO1 vector harboring "scrambled" non-coding shRNA was also prepared and used to generate lentivirus for transduction of the same primary HASM cell lines that were used to generate PUMA-deficient stable cultures.

2.14. Quantitative PCR for PUMA and NOXA mRNA

Total cellular RNA was isolated using the RNeasy Plus Mini Kit (Qiagen, Mississauga, ON) then 1 μg was reverse transcribed using the QuantiTect Reverse Transcription Kit (Qiagen, Mississauga, ON). Abundance of mRNA for PUMA and NOXA was determined with an Applied Biosystems 7500 Real-Time PCR System instrument using the Power SYBR Green PCR Master Mix (Applied Biosystems) [36]. Oligonucleotide primers were as follows: for NOXA, 5′-ATTACCGCTGGCCTACTGTG-3′ (forward) and 5′-GTGCTGAGTTGGCACTGAAA-3′ (reverse); for PUMA, 5′-CTGTGAATC-CTGTGCTCTGC-3′ (forward) and 5′-AATGAATGCCAGTGGTCACA-3′ (reverse). A dissociation curve was generated at the end of each PCR reaction to verify that a single product was amplified. The relative expression levels of genes normalized to the endogenous reference gene (18 S rRNA: primers = 5′-CGCCGCTAGAGGTGAAATTC-3′ (forward) and 5′-TTGGCAA-ATGCTTTCGCTC-3′ (reverse)) and relative to vehicle treated controls was calculated by the equation $2^{(-\Delta\Delta CT)}$. The ΔC_T value was determined by subtracting the average 18 s rRNA C_T value from the average C_T value of the corresponding target transcript. The calculation of $\Delta\Delta C_T$ values involves subtraction of the ΔC_T calibrator value (vehicle treated). For the vehicle treated samples $\Delta\Delta C_T = 0$ and 2^0 equals 1. For the simvastatin-treated samples, $2^{-\Delta\Delta CT}$ indicates the fold change in gene expression relative to time-matched controls.

2.15. Statistical analysis

The results were expressed as means ± SDE and statistical differences were evaluated by one-way or two-way ANOVA followed by Tukey's or Bonferroni's post hoc test, using Graph Pad Prism 4.0. $P<0.05$ was considered significant. For all experiments data was collected in triplicate from at least three cell lines unless otherwise indicated.

3. Results

3.1. Simvastatin induces apoptosis in human lung mesenchymal cells

We initially tested the concentration- and temporal effects of simvastatin on primary cultured HASM and HAF viability using MTT assay (Fig. 1A, B). Viability in both cell types was significantly compromised after 48 h by maximum simvastatin concentrations (20 μM), whilst the lowest concentration of simvastatin used (5 μM) was significantly toxic (~25%) only after 96 h; the maximum effect caused by 20 μM simvastatin at this time point exceeded 50%. As we used multiple primary human airway mesenchymal cells of relatively low passage number we did observe some degree of biological variation in the magnitude of the simvastatin effect, however all cell lines exhibited the same trend in response. Concomitant with reduced viability, loss of spindle-shaped mesenchymal cell morphology, and the appearance of features of apoptosis (e.g. cell rounding, shrinkage, partial detachment) were observed (Fig. 1C). Apoptotic cell death was confirmed by flow cytometry detection of hypodiploid nuclei (Fig. 1D, F, G)) in HASM and HAF. Laser scanning cytometry was used for further confirmation of simvastatin-induced apoptosis based on analysis of nuclear DNA content, condensation and nuclear morphology (Fig. 1E). These data demonstrate simvastatin induces apoptosis in primary cultured human lung mesenchymal cells.

3.2. Inhibition of the mevalonate cascade but not cell cholesterol depletion drives apoptosis

In cancer cells statin-induced apoptosis is due to the loss of cell membrane cholesterol and/or depletion of polyisoprene cholesterol precursors, FPP and GGPP, essential lipid anchors for active small GTPase proteins [37,38]. Thus, we investigated the effect of: (*i*) simvastatin treatment on *de novo* synthesis and total cellular cholesterol content, (*ii*) replacement of cholesterol intermediates on apoptosis induced by HMG-CoA reductase inhibition, and (*iii*) simvastatin exposure on membrane anchoring of small GTPases. Simvastatin markedly diminished *de novo* cholesterol synthesis in HASM and HAF (Fig. 2A) but not total cellular cholesterol (Fig. 2B) over 96 h of treatment. In subsequent experiments we measured the effect of adding mevalonate, FPP or GGPP on simvastatin-induced apoptosis. For these and similar studies described hereafter, we completed preliminary experiments (not shown) to assess concentration-response effects of mevalonate (0–10 mM), FPP (0–30 μM), and GGPP (0–30 μM) in the absence of simvastatin to identify the highest concentration that could be used

without affecting cell viability; in doing so we determined that the maximum concentration of each compound we could use whilst maintaining normal cell viability was 2 mM for mevalonate, and 7.5 μM for FPP and GGPP. Using these conditions we found that while there was no effect of mevalonate, FPP and GGPP on cell viability, these compounds were sufficient to prevent any statistically significant loss of cell viability when simvastatin was added concomitantly (Fig. 2C–E) ($p>0.05$). These data suggest that depletion of mevalonate cascade intermediates, but not cholesterol itself, is linked to simvastatin-induced apoptosis. As Ras small GTPases require geranylgeranylation or

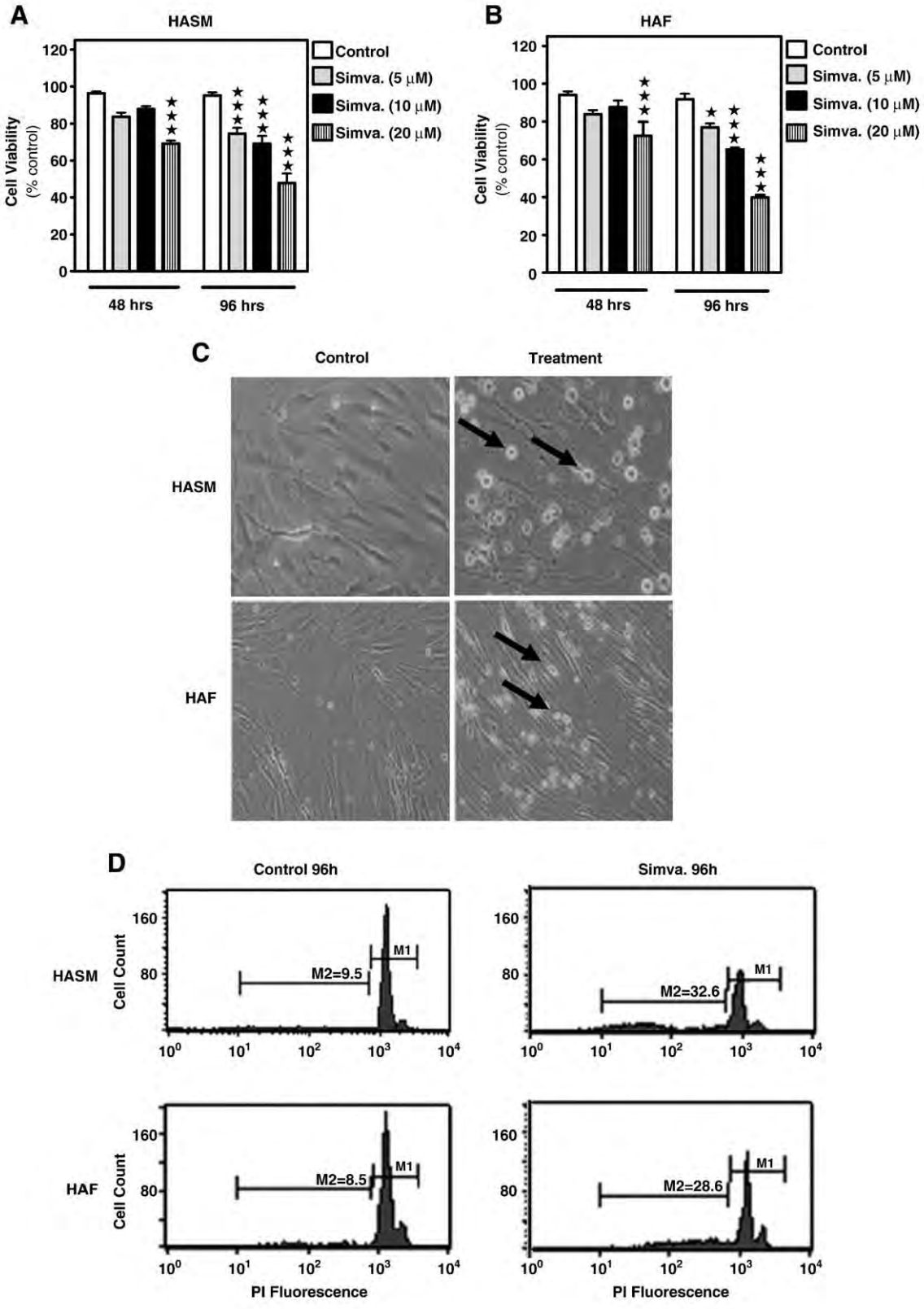

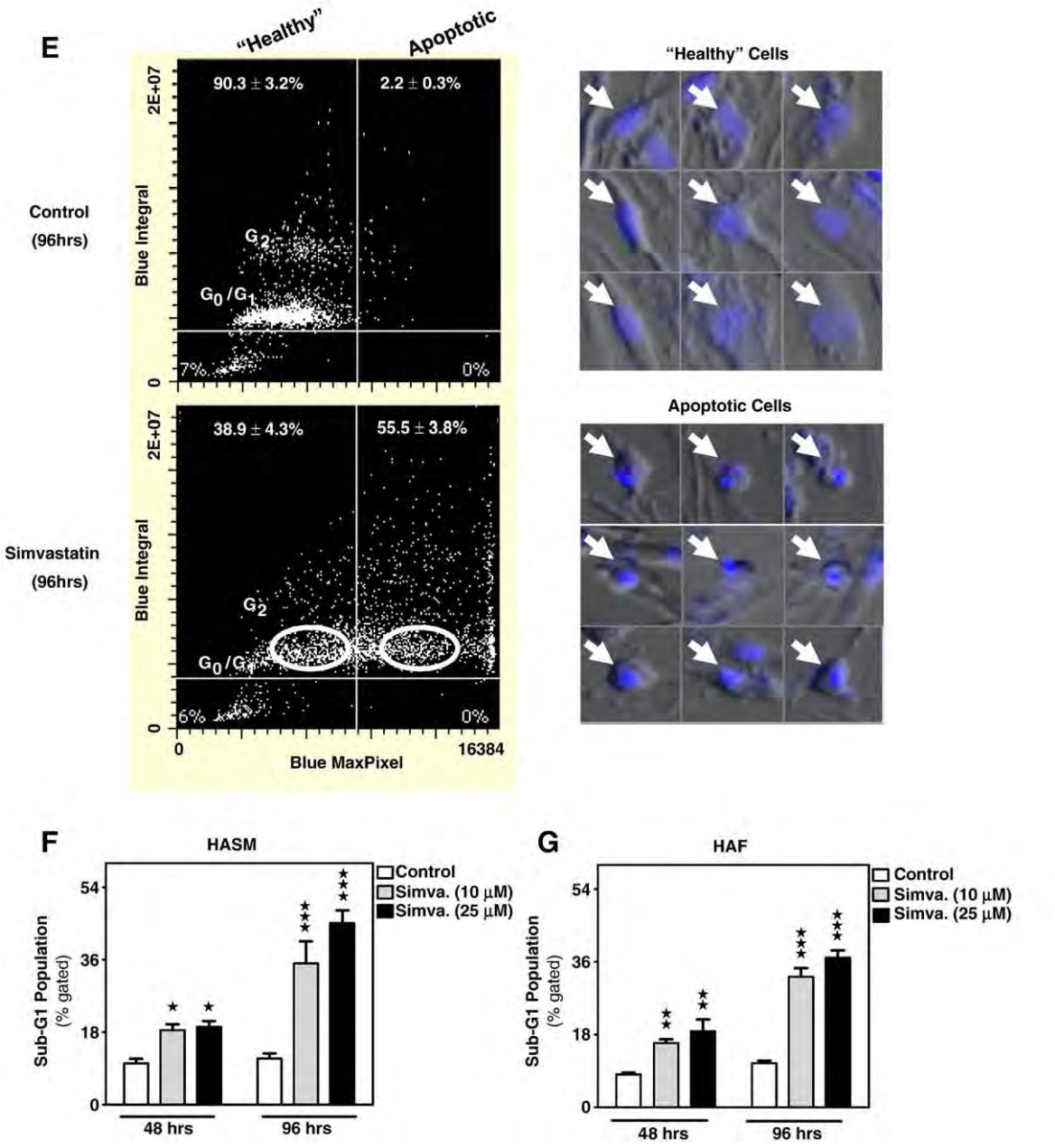

Fig. 1. Simvastatin induces apoptosis in primary human airway smooth muscle (HASM) cells and airway fibroblasts (HAF). (A, B) The cells were treated with simvastatin (5, 10 or 20 μM) and cell viability was assessed 48 and 96 h thereafter by MTT assay. Control cells for each time point were treated with the solvent control (DMSO). Results are expressed as percentage of corresponding time point control and represent the means ± SD of 12 independent experiments in three different sets of patient-matched HASM and HAF (*P<0.05; **P<0.01; ***P<0.001). (C) HASM and HAF cells treated with 10 μM simvastatin for 96 h were then photographed under phase contrast microscopy settings. Arrows indicate partially detached cells with condensed morphology. (D) Examples of typical DNA histograms showing propidium iodide staining measured by flow cytometry for control and simvastatin-treated HASM and HAF. In each panel the region labeled "M2" indicates cells with sub-diploid DNA and the percentage of cells within those regions are indicated. Peaks for diploid (G1) and tetraploid (G2) nuclear staining in non-apoptotic cells are visible in the region labeled as "M1". HASM (top row) and HAF (bottom row) cells were treated with DMSO (control, left column) or 10 μM simvastatin for 96 h (right column). (E) Examples of typical scattergrams obtained by LSC of HASM cells treated with vehicle control or 10 μM simvastatin for 96 h. Y-axis data represents total integrated fluorescence of individual events (nuclei) and X-axis show maximum pixel fluorescence intensity within each event contour. Horizontal line in each scattergram represents the threshold determined for reliable event identification, and the vertical line represents the outer boundary for normal cell pixel intensity (determined from control data). The position of cells with diploid or tetraploid nuclear DNA, representing G_0/G_1 or G_2 cell cycle phase, is indicated in each scattergram. Percentages shown in upper quadrants indicate the mean% of cells determined from three separate experiments ± SD. Images on the right are galleries of images for individual cells (indicated by white arrows) representing events indicated within the circled regions of the scattergram for simvastatin treatment, indicating "healthy" and "apoptotic" G_0/G_1 cells. (F and G) Percent sub-G1 HASM and HAF abundance induced by simvastatin (10 or 25 μM) or DMSO solvent control after 48 and 96 h. Results represent the means ± SD of 6 independent experiments in two different patient-matched HASM and HAF primary cell lines. *P<0.05; and ***P<0.001 compared to time-matched control.

farnesylation for plasma membrane insertion and activation, we next used immunoblotting to assess the effects of HMG-CoA reductase inhibition on sub-cellular distribution of small GTPases. Simvastatin treatment markedly depleted Rac1/2/3 and RhoA from membrane-fractions, resulting in their enrichment in the cytosol (Fig. 2F).

3.3. The intrinsic apoptotic pathway is selectively activated by simvastatin

In various cancer cell lines both extrinsic and the intrinsic apoptotic pathways can be induced by statins [18,20,39]. Thus, we

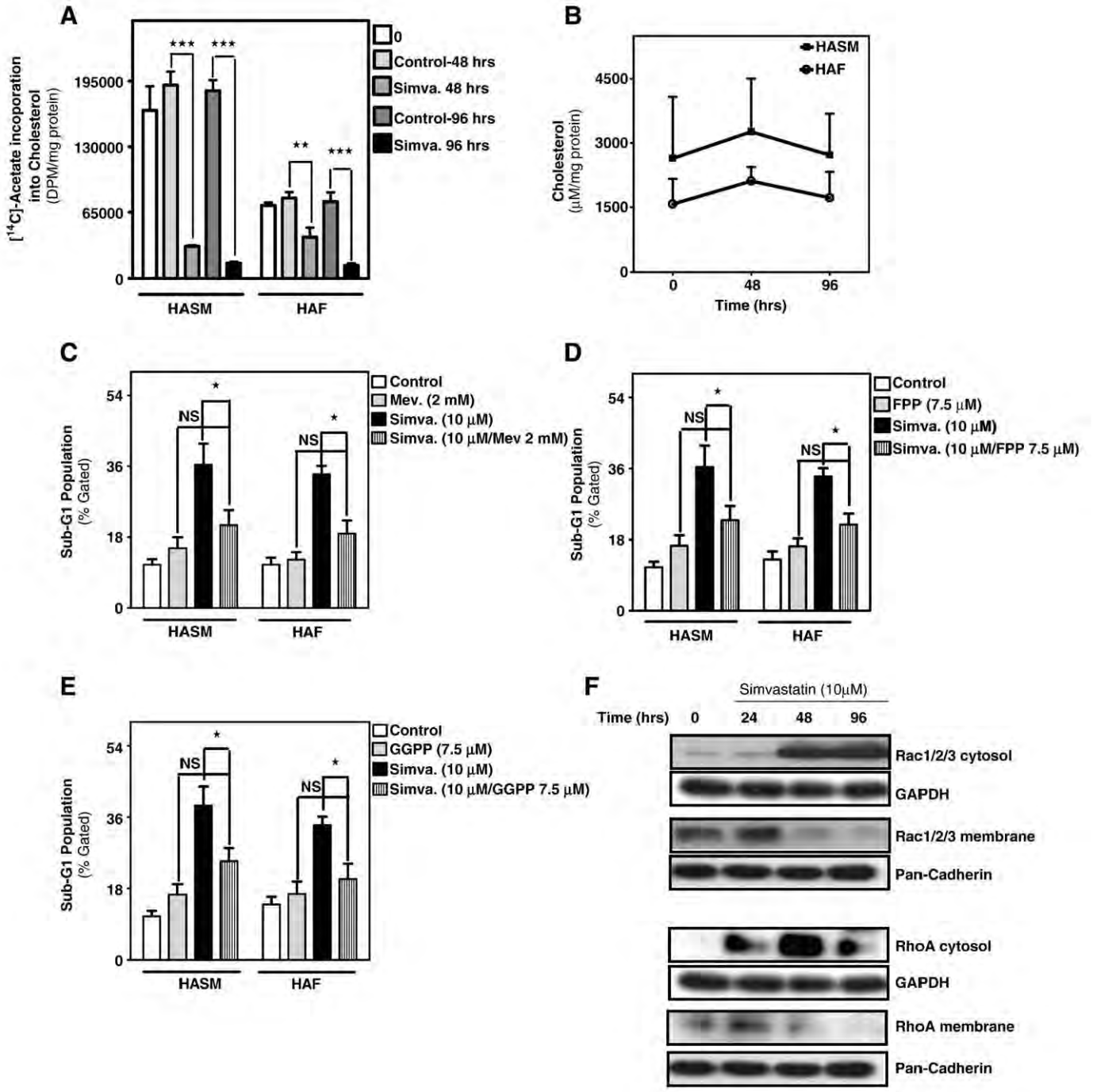

Fig. 2. Simvastatin induces apoptosis in airway mesenchymal cells via effects on isoprenoid precursors of cholesterol. (A) Simvastatin inhibits *de novo* cholesterol biosynthesis in HASM and HAF. Figure shows 96 h time course of simvastatin (10 μM) effects on [^{14}C] acetate incorporation using thin-layer chromatography assay for cholesterol synthesis. For each time point, the treated cells were compared with control cells, which were treated with culture medium and simvastatin solvent (DMSO). Results are expressed as the means ± SD of 9 independent experiments in three different sets of HASM and HAF (HASM and HAF were from the same individuals). $^{**}P<0.0$; and $^{***}P<0.001$ compared to time-matched control. (B) 96 h time course of simvastatin (10 μM) effects on total cholesterol content of HASM and HAF. Cholesterol was measured by a fluorescence-based assay. Cholesterol content at 48 and 96 h was compared with cells prior to simvastatin treatment ($t=0$ h). Results are shown as units of cholesterol (based on a standard curve) normalized to total cellular protein in cell lysates and represent the means ± SD of 9 independent experiments in three different patient-matched HASM and HAF primary cell lines. (C–E) Effects of supplementation with 2 mM mevalonate (C), 7.5 μM FPP (D), or 7.5 μM GGPP (E) 4 h prior to treatment with simvastatin (10 μM, 96 h) on apoptosis (percentage of hypo-diploid HASM and HAF), measured by flow cytometry after staining with propidium iodide. For each experiment control cells were treated with simvastatin solvent (DMSO) alone (control) or with both DMSO and the appropriate solvent for each cholesterol precursor (i.e. ethanol for "mevalonate control" and DMSO for "FPP control" and "GGPP control"). Results are expressed as mean ± SD of 9 independent experiments using three different patient-matched HASM and HAF primary cell lines. $^{*}P<0.05$, simvastatin-treated compared to simvastatin with mevalonate, FPP or GGPP; NS — $P>0.05$, mevalonate, FPP or GGPP treated compared to simvastatin treated in the presence of mevalonate, FPP or GGPP. (F) Time course of simvastatin (10 μM) on the abundance of Rac1/2/3 and RhoA in membrane and cytosolic fractions obtained from HASM (Western blot). GAPDH abundance was assessed to control for loading in cytosolic fractions, and to confirm lack of cytosolic contamination in membrane fractions (not shown). Pan-cadherin abundance was used to normalize for loading of membrane fractions. Data are typical of 3 independent experiments using different primary cultures.

investigated the involvement of apoptotic cascades in HASM and HAF after simvastatin treatment. The extrinsic apoptotic pathway was not activated, as neither pro-caspase-8 nor its substrate, the pro-apoptotic Bcl-2 protein, BID, were cleaved (Fig. 3A, B). In contrast, 10 μM simvastatin induced time-dependent accumulation of cleaved caspase-9, cleaved caspase-7 and -3, and their catalytic product, cleaved poly ADP-ribose polymerase-1 (PARP-1) in HASM (Fig. 3C) and HAF (Fig. 3D). The enzymatic activity of caspase-8, -9, and -3/7 was also verified by luminometric Caspase-Glo® assay (Fig. 3E, F), and confirmed simvastatin did not induce caspase-8 activity but did significantly induce catalytic activity of caspase-3/7 and caspase-9. These results provide evidence that simvastatin-induced apoptosis is selectively triggered via the intrinsic pathway.

3.4. Simvastatin triggers apoptosis via p53-dependent upregulation of PUMA

The tumor suppressor protein p53 executes complex control over apoptosis, senescence, and cell proliferation by regulating transcription and cytosolic function of Bcl-2 family members including, Bax and BH3-only members, PUMA and NOXA [40,41]. We investigated the temporal impact of simvastatin on abundance of p53, and selected p53-regulated proteins. In HASM cells PUMA, NOXA, and Bax protein were significantly increased after 96 h simvastatin exposure. We also noted an increase of phosphorylated forms of p53 (phosphorylated serines 15 and 37, Fig. 4A) that accompany p53 activation [42]. To assess the dependence of these effects of inhibition of HMG-CoA

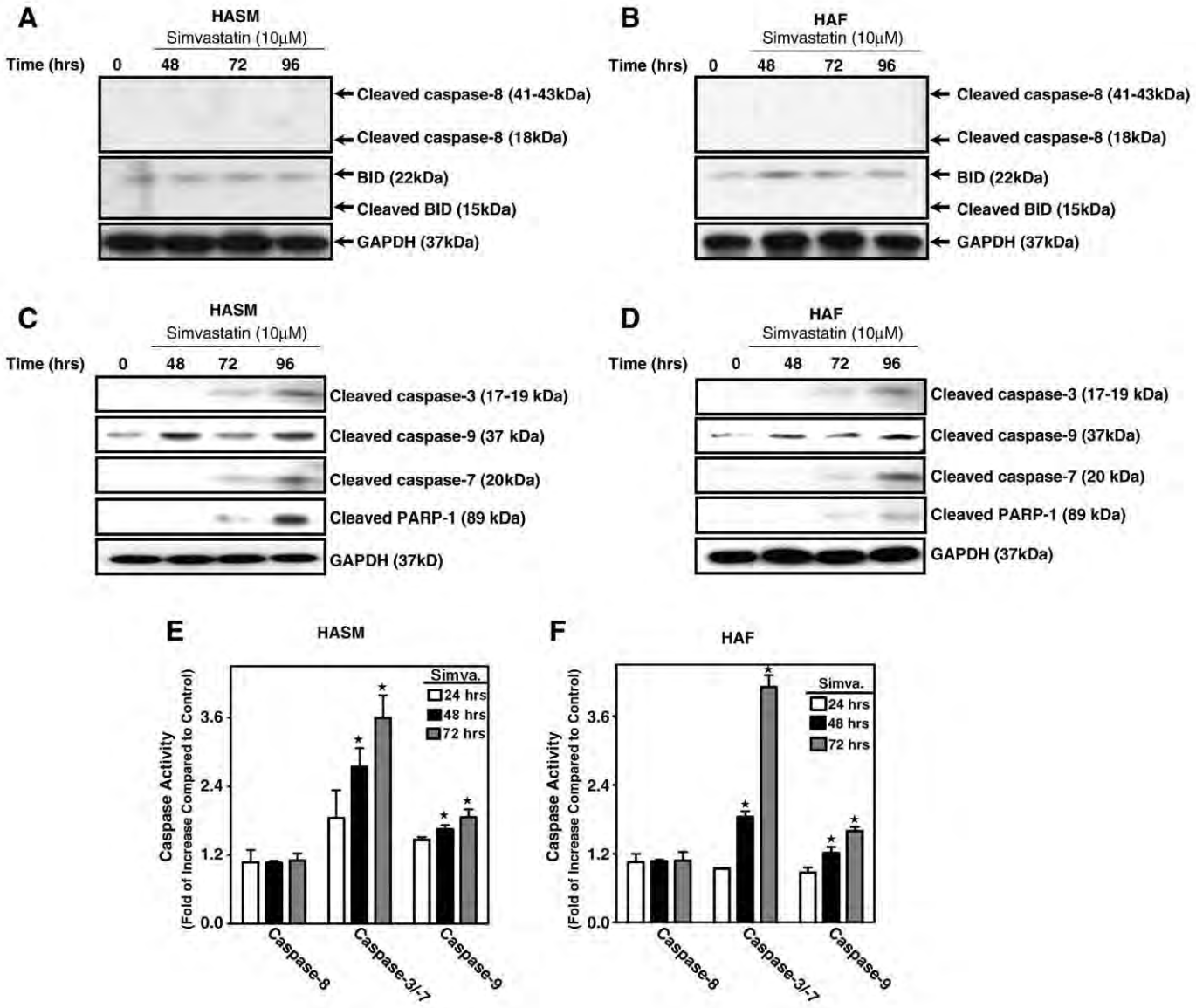

Fig. 3. Simvastatin induces HASM cell and HAF apoptosis via the intrinsic cell death pathway. (A, B) Immunoblot detection of cleaved caspase-8 and its downstream substrate BID, in total cell lysates of primary cultured HASM (A) and HAF (B). Cells were treated with simvastatin (10 μM) for up to 96 h. Positions and approximate molecular weight of predicted and visible protein signals are indicated by arrows. For all lanes GAPDH was used as protein loading control. Blots are typical of three experiments completed using different patient-matched cultures of HASM and HAF. (C, D) Immunoblots for cleaved caspase-3, -9, -7 and downstream substrate, PARP-1 in total cell lysates of primary cultured HASM (C) and HAF (D) cells treated with simvastatin (10 μM) for up to 96 h. For all lanes GAPDH was used as protein loading control. Blots are typical of thee experiments completed using different patient-matched cultures of HASM and HAF. (E, F) Effects of simvastatin (10 μM) treatment (up to 72 h) on caspase-8, caspase-3/7, and caspase-9 enzymatic activity, as detected by Caspase-Glo® luminometric assay. Caspase activity normalized to that measured for solvent-only treated cultures is represented on the Y-axis. The data represent mean ± SD of duplicate experiments performed on 4 different patient-matched primary HASM and HAF cell lines. *$P<0.05$ compared to untreated controls.

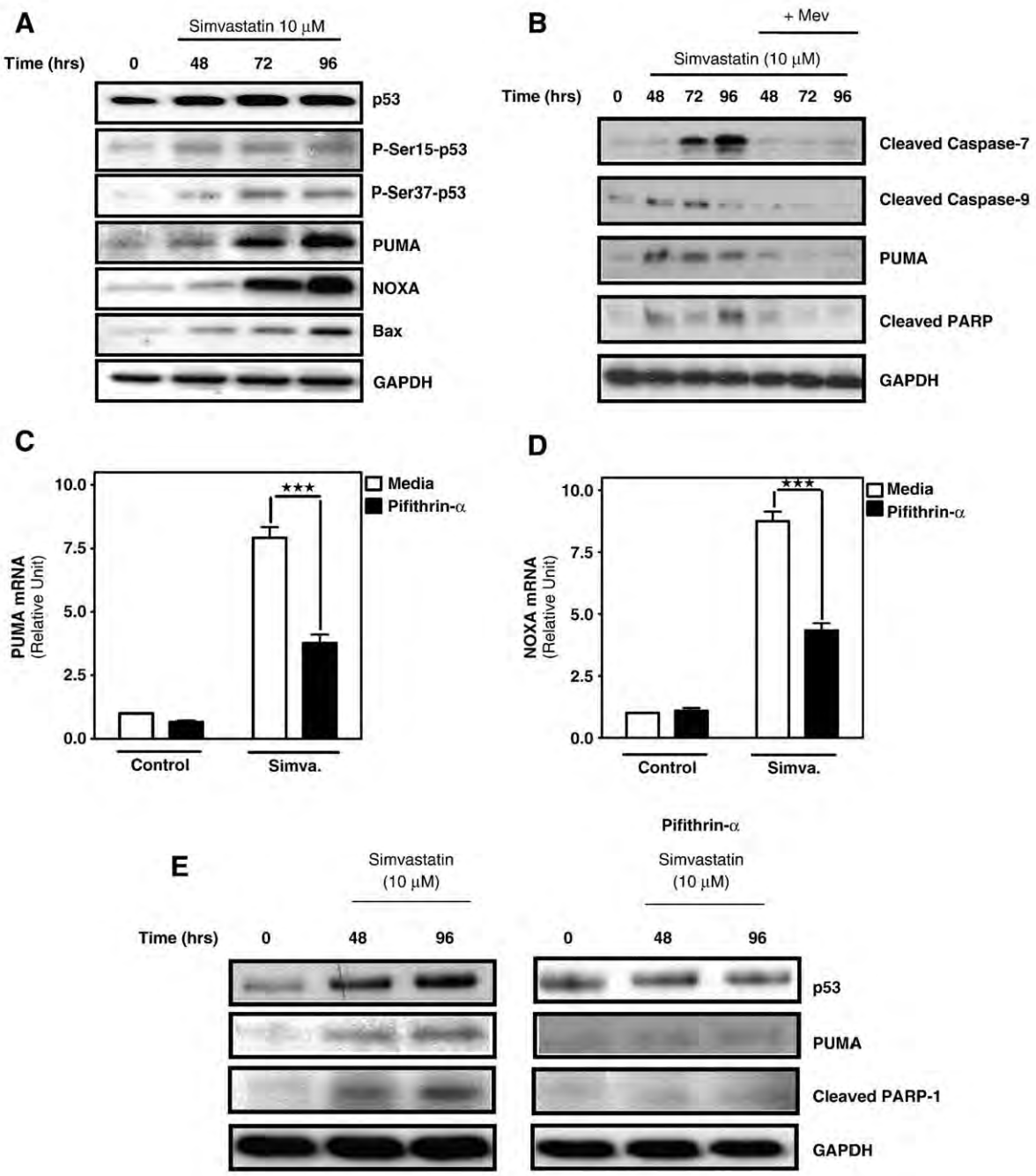

Fig. 4. Simvastatin-induced apoptosis in HASM and HAF involves a p53 death pathway. (A) Accumulation of cell death-related proteins transcriptionally regulated by p53 (Western blot). HASM cells were treated with simvastatin (10 μM) for up to 96 h as indicated. Immunoblot was performed using total cell extracts resolved by SDS-PAGE. GAPDH was used as loading control for all experiments. Shown data are typical of 4 independent experiments. Legend: P-Ser15-p53 — p53 with phosphorylated serine 15; P-Ser37-p53 — p53 with phosphorylated serine 37. (B) Mevalonate inhibits simvastatin-induced caspase-7, -9, and PARP cleavage and PUMA expression. HASM cells were pre-treated with mevalonate (2 mM, 4 h) and then co-treated with simvastatin (10 μM) for indicated time points. Immunoblot was done using total cell extracts resolved by SDS-PAGE. GAPDH was used as a loading control for all experiments. Blots are typical of 2 independent experiments. (C and D) Effect of p53 inhibition with cyclic pifithrin-α on PUMA and NOXA expression in simvastatin-treated cells. HASM cells were pre-treated with cyclic-pifithrin-α (4 h, 10 μM) before simvastatin exposure (10 μM) for 96 h. Total RNA was extracted and qRT-PCR performed to measure PUMA (B) and NOXA (C) mRNA abundance relative to the internal maker, 18 S RNA. Data were obtained in triplicate from two cell lines. *** — $P<0.001$compared to time-matched untreated samples. (E) Cyclic pifithrin-α inhibits PUMA accumulation and PARP-1 cleavage in simvastatin-treated HASM cells. Cultures were pre-treated with cyclic-pifithrin-α (10 μM, 4 h) before simvastatin exposure (10 μM) for up to 96 h. Immunoblottings for p53 (53 kDa), PUMA (23 kDa) and cleaved PARP-1 (89 kDa) were performed using total cell extracts resolved by SDS-PAGE. GAPDH was used as loading control for all experiments. Blots shown are typical of 4 independent experiments. (F) Inhibition of p53 decreases simvastatin-induced cell death. Where indicated HASM cells were pre-treated with cyclic-pifithrin-α (5 or 10 μM, 4 h) prior to simvastatin (10 μM) co-treatment for an additional 60 or 96 h. Cell viability was assessed using MTT assay. Data shown are the mean of 12 experiments performed in quadruplicate. * — $P<0.05$ compared to time-matched cultures treated with simvastatin alone; ** — $P<0.01$ compared to time-matched cultures treated with simvastatin alone. (G) Preparation of HASM cell lines refractory to simvastatin-induced PUMA accumulation using lentivirus-delivered shRNAi. HASM were transduced with lentivirus harboring PUMA-selective or non-coding scrambled shRNAi, and stable cell lines were generated using puromycin selection. Cell cultures were treated with simvastatin (10 μM) for up to 96 h, then total protein was detected for PUMA. There was not any detectable PUMA in Simvastatin-treated cells which were infected with PUMA shRNAi. (H) Inhibition of PUMA expression decreases simvastatin-induced cell death. Wild type HASM cell cultures or those transduced with PUMA or non-coding shRNAi were treated with simvastatin (10 μM) for 96 h then cell viability was assessed using MTT assay. Data shown are the mean of 12 experiments performed in quadruplicate using three different primary lines. * — $P<0.05$ compared to time-matched scrambled shRNAi-transduced cultures.

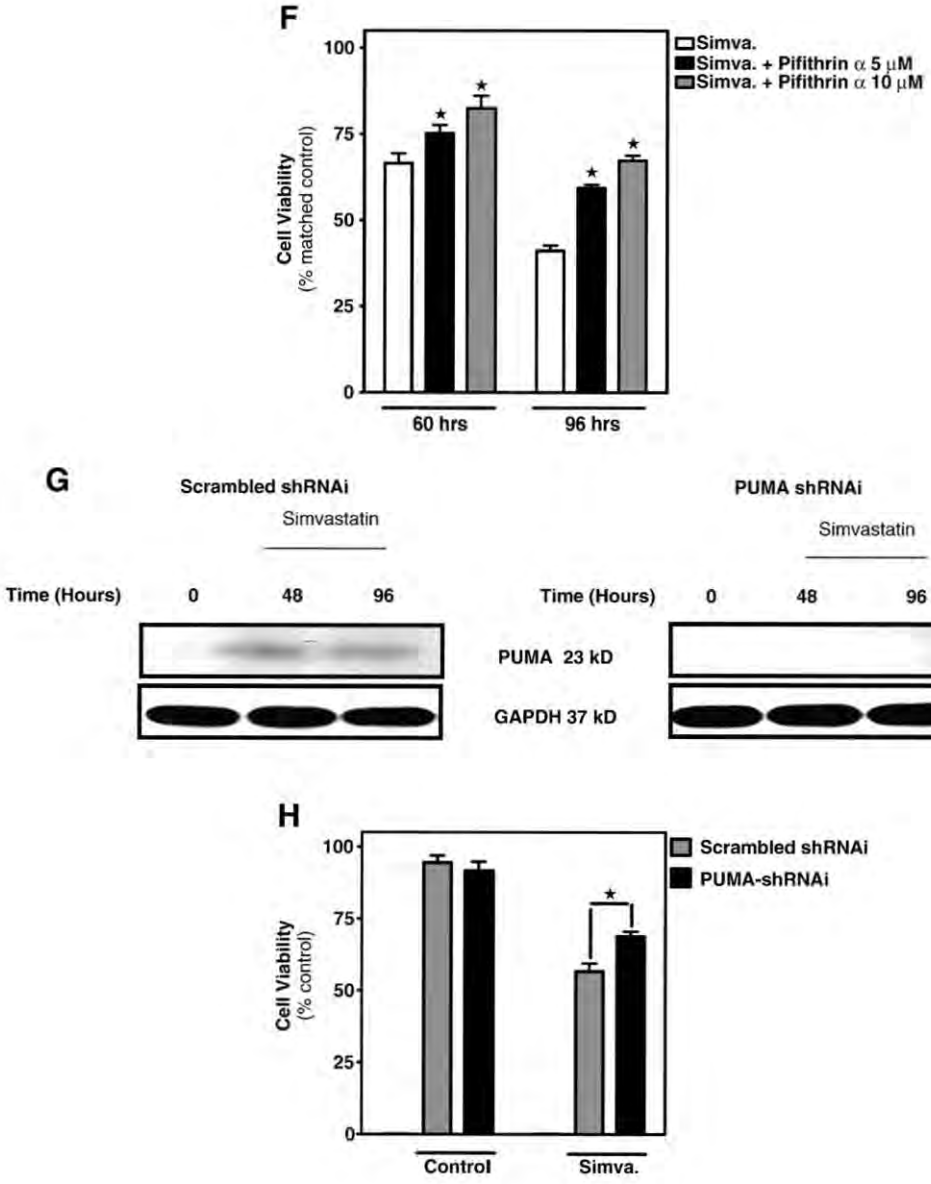

Fig. 4 (*continued*).

reductase, we co-treated cells with simvastatin and mevalonate. Addition of mevalonate was sufficient to block caspase-9 and -7 cleavage, PUMA expression and PARP cleavage (Fig. 4B). To confirm the involvement of p53 in simvastatin-induced accumulation of BH3-only proteins, we examined the effects of the p53-transcriptional inhibitor, cyclic-pifithrin-α [43], on simvastatin-induced accumulation of mRNA for PUMA and NOXA. Simvastatin treatment induced a 7–8-fold increase in PUMA and NOXA after 96 h (Fig. 4C, D), whereas p53 inhibition suppressed this response by nearly 60% (Fig. 4C, D). We observed a similar suppression of simvastatin-induced accumulation of PUMA and cleaved PARP-1 (Fig. 4E). Importantly, p53 inhibition with cyclic-pifithrin-α also significantly inhibited, but did not fully prevent, simvastatin-induced cell death in HASM cells (Fig. 4F).

The best understood pathway for p53-induced apoptosis involves PUMA, which is transcriptionally induced by p53 and once translated, binds Bcl-xL to permit cytoplasmic p53-facilitated formation of mitochondrial permeability pores by Bax [13,40]. Therefore we tested whether PUMA is required for simvastatin driven lung mesenchymal cell apoptosis. We developed a lentiviral vector with puromycin selection cassette that encodes shRNA for human PUMA and transduced HASM cell to establish stable silencing of PUMA. Our initial experiments confirmed that the cell cultures generated were refractory to simvastatin-induced PUMA expression, whereas control cultures expressing a non-coding scrambled shRNA exhibited PUMA protein accumulation upon simvastatin exposure (Fig. 4G). We measured cell viability of PUMA-null mesenchymal cells in response to simvastatin and found that whereas wild type primary HASM and cultures transduced with scrambled shRNA exhibited a 45–50% loss of viability after 96 h, cell cultures deficient in PUMA were significantly less prone, but not fully protected from simvastatin-induced cytotoxicity (Fig. 4H).

3.5. Simvastatin induces mitochondrial membrane permeability and ROS formation

To determine the biologic significance of p53-dependent PUMA and NOXA upregulation by simvastatin, we next tested if simvastatin exposure affected mitochondrial function in HASM cells and HAF. We

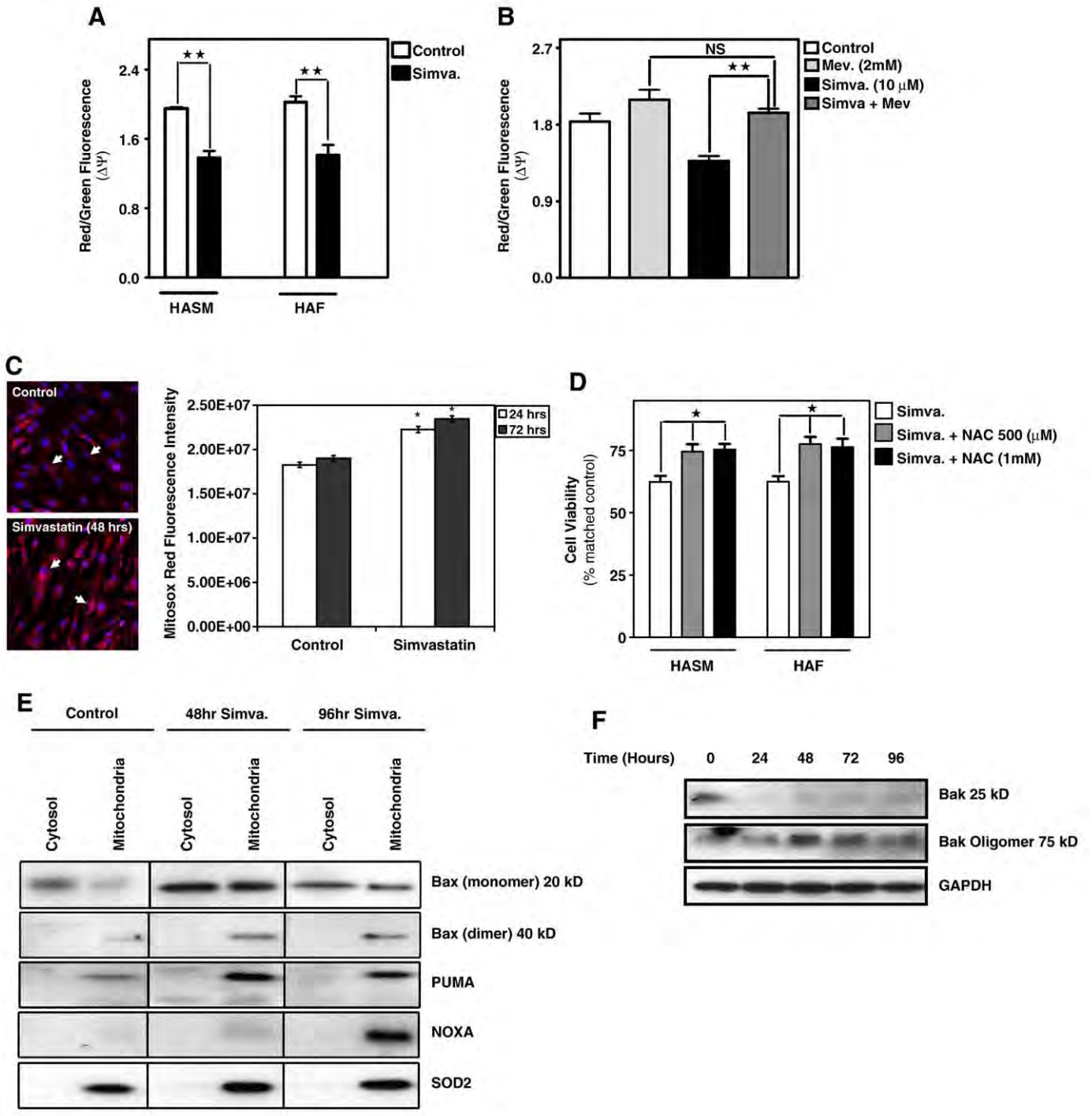

Fig. 5. Simvastatin-induced apoptosis in primary HASM and HAF involves mitochondria dysfunction and permeability pore formation. (A) Effects of simvastatin treatment (10 μM, 48 h) on mitochondrial trans-membrane potential ($\Delta\Psi_m$). After simvastatin treatment cells were loaded with JC-1 dye and the potential-dependent accumulation in the mitochondria (reduced $\Delta\Psi_m$ indicated by a decrease in Red:Green fluorescence) measured directly (spectrofluorometry). Data represent the average values from triplicates of three independent experiments. * — $P<0.05$ compared to time-matched solvent-only treated controls. (B) Using an experimental design similar to 5A, in another experiment HASM cells were pre-treated with mevalonate (2 mM, 4 h) and then co-treated with simvastatin (10 μM, 48 h). Mevalonate significantly inhibited effect of simvastatin on $\Delta\Psi_m$ decrease ($P<0.05$). (C) Effects of simvastatin (10 μM, 24 and 72 h) on mitochondrial reactive oxygen species (ROS) generation in HASM cells. ROS was measured by laser scanning cytometry in cells stained with Mitosox Red and the DNA dye H33342. Typical images obtained are shown on the left (arrows indicate typical staining of individual cells; ROS staining is red, nuclear staining is blue). Average cellular ROS levels were determined from 200 fields in triplicate slides prepared from two different cell cultures. Histogram (Y-axis) shows fold elevation in cellular ROS compared to time-matched, vehicle-only treated controls. * — $P<0.05$ compared to time-matched vehicle-only controls. (D) Histogram showing effects of NAC on simvastatin (10 μM, 96 h) induced cell death in HASM and HAF. HASM and HAF pre-treated with indicated concentration of NAC for 4 h and then co-treated with simvastatin with indicated concentration and time point. Data represent the average values from quadruplicates of two independent experiments. * — $P<0.05$ compared to time-matched vehicle- or NAC only controls. (E) SDS-PAGE/immunoblots showing the change in the relative cytosolic and mitochondrial distribution of Bax monomer (20 kDa), Bax dimer (40 kDa), PUMA, and NOXA after simvastatin treatment (10 μM, 48 and 96 h). Cytosol and mitochondrial membrane fractions were obtained as described in Section 2 then subjected to immunoblotting. Fraction purity and sample loading was monitored by immunoblotting for MnSOD2 protein. (F) Non-reducing PAGE/immunoblot analysis of Bak monomers (25 kDa) and 75 kDa oligomers in whole cell lysates from HASM treated with simvastatin (10 μM) for up to 96 h. Equal protein loading was confirmed using GAPDH.

measured $\Delta\Psi_m$ upon simvastatin treatment using the ratiometric fluorescent indicator, JC-1 and found a marked decrease in $\Delta\Psi_m$ (Fig. 5A). Notably, as we observed for effects of simvastatin on cleavage of caspase-7, -9 and PARP, and PUMA expression, the addition of exogenous mevalonate significantly inhibited simvastatin-induced suppression of $\Delta\Psi_m$, confirming that depletion of mevalonate cascade intermediates downstream from HMG-CoA reductase activity underpins disruption in mitochondrial function (Fig 5B). Using the ROS-sensitive dye MitoSox Red, we also observed that there is a marked increase in mitochondria-derived ROS generation compared to corresponding controls ($P<0.05$) after 24 and 72 h of simvastatin exposure (Fig. 5C). These data implicate involvement of mitochondria in simvastatin-induced lung mesenchymal cell death, an observation strengthened by the fact that N-acetyl-L-cysteine (NAC), a broad range ROS scavenger [28], partially inhibited simvastatin-induced cell death (Fig. 5D). To test whether the loss of $\Delta\Psi_m$ was caused by simvastatin-induced pore formation in mitochondrial membrane we next tested the association of pro-apoptotic Bcl-2 family members with mitochondria. Simvastatin caused marked enrichment of mitochondrial PUMA, NOXA, and both monomeric and dimerized Bax (Fig. 5E). Also within 24 h of treatment, simvastatin induced oligomerization of Bak that was sustained through 96 h of treatment (Fig. 5F). Collectively these observations confirm that simvastatin causes significant disruption of mitochondrial function, including the formation of membrane permeability pores, thus creating the potential for the release of proteins that promote apoptosis.

3.6. Simvastatin induces selective release of mitochondrial IAP inhibitor proteins

To further examine the effect of simvastatin on mitochondria, we monitored the release of various factors associated with the mitochondrial death pathway. We first examined the mitochondrial apoptosis initiating factor (AIF), a FAD-dependent oxidoreductase [44], and the mitochondrial nuclease, endonuclease G (Endo G) [34]. When released these proteins translocate to the nucleus to initiate DNA damage. Using confocal imaging we observed AIF and Endo G in mitochondria, but saw no evidence for AIF or Endo G in cell nuclei after treating HASM and HAF with simvastatin (10 μM, 72 h) (Fig. 6A, B). In a parallel experiment in which we employed biochemical fractionation of mitochondria we did observe a marked cytosolic accumulation of two mitochondrial proteins, Smac/DIABLO and Omi/HtrA2, which block IAP proteins (Fig. 6C). In striking contrast, in the same experiment we were unable to detect release of cytochrome *c* from mitochondria. This suggests that the activation of caspase-9 by simvastatin treatment (Fig. 3) occurs independently of apoptosome formation. To more directly assess whether simvastatin-induced caspase-9 activation occurs in the absence of apoptosome formation we compared simvastatin-induced caspase-9 activity in the presence and absence of the apoptosome formation inhibitor NS3694. Apoptosome inhibition had no effect on the effects of simvastatin, as caspase-9 activity increased approximately 1.8-fold, similar to the effect in Fig. 3E and F, in HASM cells and in HAF (not shown) (Fig. 6D), thus, confirming that mitochondrial release of cytochrome *c* is not a principal mechanism in simvastatin-induced cell death.

As our findings implicate a significant role for Smac and Omi in statin provoked cell death, we next tested whether Smac can potentiate simvastatin-induced apoptosis and caspase-9 activation by measuring the impact of an exogenous N7-Smac mimetic peptide that contains the 7 terminal amino acid–IAP-binding motif [45]. Notably, we observed that though treatment with the N7-Smac peptide alone showed little effect on caspase-9 activity, it did strongly potentiate simvastatin-induced caspase-9 activation and cell death (Fig. 6E, F). These observations indicate that mitochondrial release of Smac contributes to cell death-triggered by simvastatin treatment.

3.7. Simvastatin treatment disrupts mitochondrial fission

Electron microscopy of simvastatin-treated lung mesenchymal cells revealed profound effects on mitochondrial morphology. Mitochondria in simvastatin-treated HASM cells and HAF exhibited an atypical stretched forkhead morphology that in other systems has been identified as a feature linked to the inhibition of mitochondrial fission (Fig. 7A) [16]. As mitochondria are dynamic organelles that move, fuse and divide, disruption of these activities has been associated with cell dysfunction and death [46,47]. Moreover, we and others have reported that the inhibition of mitochondrial fission promotes release of Smac, but not cytochrome *c*, and leads to Bax/Bak-dependent apoptosis [16,47,48]. Thus, to better determine whether mitochondrial fission is compromised by simvastatin, we isolated mitochondria and used immunoblotting to examine the subcellular distribution of dynamin-related protein 1 (Drp1), an essential component of the mitochondria-associated protein complex that underpins mitochondrial division [49]. Our findings show that though simvastatin increased Drp1 expression in HASM and HAF it also promoted a virtually complete loss of mitochondria-associated Drp1 with concomitant accumulation of inactive protein in the cytosol (Fig. 7B, C). These observations suggest that the selective release of Smac and Omi induced by simvastatin (Fig. 6C) may be related to the suppression of mitochondrial fission.

4. Discussion

As statins are widely used and have broad positive health benefits beyond their cholesterol-lowering capacity [50], a full understanding of their mechanism of action is needed. Consistent with previous studies, we show that statin-induced cell death in normal somatic cells is mediated by depletion of isoprenoids [5,6,51,52]. Our study also has several unique features and significantly extends current understanding of downstream mechanisms for statin-induced apoptosis in otherwise healthy cells. New data conclusively point to mitochondrial mechanisms and intrinsic apoptosis signaling in statin-induced mesenchymal cell death. We reveal the involvement of p53 and its induction of BH3-only protein expression to promote mitochondrial permeability pore formation involving Bax and Bak. Moreover, we show for the first time that mitochondria-derived ROS are induced by statins and contribute to mesenchymal cell death. A particularly novel aspect of this study hinges on evidence for mitochondrial release of IAP inhibitors, Smac and Omi, in the absence of cytochrome *c* release to trigger caspase activation leading to cell death. Furthermore, we show new evidence that statin exposure is associated with disrupted mitochondrial fission; consistent with studies using different compounds and cell types [16,47,48], this is likely a critical determinant of selective IAP inhibitor release. Our use of primary cultured human lung mesenchymal cells is also unique and important, both because to date cancer cell lines have chiefly been used to investigate statin-triggered cell death pathways, and the accumulation of HASM cells and HAFs is a significant underpinning of obstructive lung diseases, which appear to respond well to statin therapy [23–25].

We show that simvastatin inhibits *de novo* synthesis of cholesterol in HASM and HAF, which is consistent with studies showing HMG-CoA reductase inhibition suppresses the incorporation of [^{14}C]-acetate into newly synthesized sterols [53]. Our observation that cellular cholesterol content was unaffected despite suppression of *de novo* synthesis for several days is somewhat paradoxical, but it is important to note that we included 0.5% FBS in culture media and that cells of mesenchymal origin have a high intrinsic capacity to take-up sterols [54]. Thus, HASM cells and HAF likely incorporate sufficient cholesterol from FBS in culture media to compensate for suppression of intracellular cholesterol biosynthesis. Inhibition of HMG-CoA reductase does lead to depletion of mevalonate and downstream metabolites, GGPP and FPP, which are

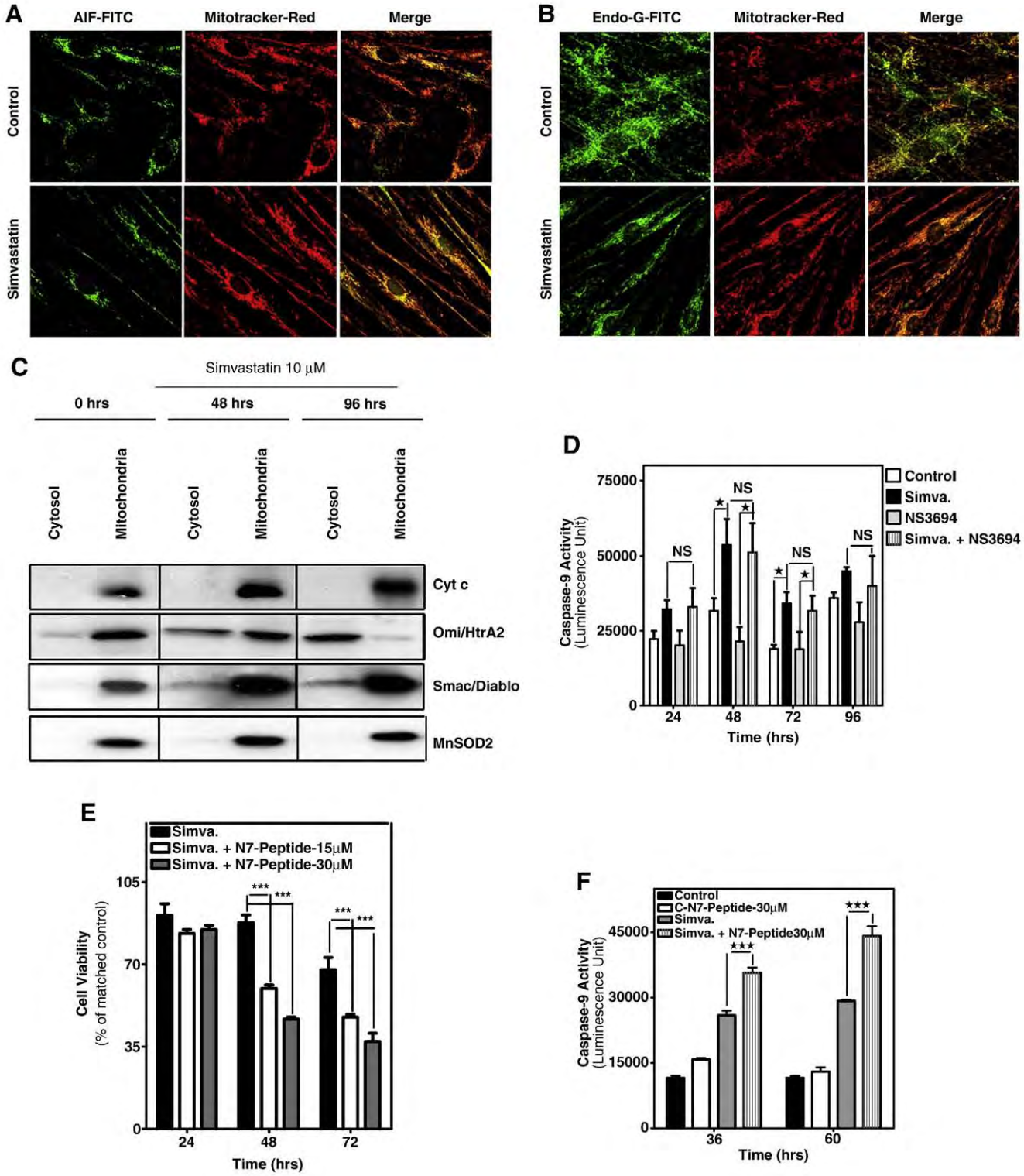

Fig. 6. Simvastatin induces selective release of Smac and Omi. (A and B) Confocal microscopy assessment of subcellular distribution of AIF (A) and Endo G (B) in HASM treated with simvastatin (10 μM, 72 h). AIF and Endo G were labeled with FITC-conjugated antibodies (green fluorescence, left panel). Cells were stained with Mitotracker Red (red fluorescence, middle panel) to indicate the position of mitochondria. Images showing AIF (A) or Endo G (B) signal merged with mitochondrial staining are shown in the right panel. White arrows indicate nuclei in representative cells. (C) Western blot analysis of cytosolic and mitochondrial fractions obtained from simvastatin-treated (10 μM, 48 and 96 h) HASM cells. Proteins assessed include cytochrome *c* (14 kDa), Omi/HtrA2 (50 kDa), and Smac/DIABLO (25 kDa). Fraction purity and equal sample loading was confirmed by probing for MnSOD2 (21 kDa). (D) Caspase-9 activity (luminometry) in HASM cells treated with simvastatin (10 μM) for up to 96 h in the presence and absence of apoptosome inhibitor, NS3694 (40 μM). Data shown are the mean of 12 experiments performed in quadruplicate. * — $P<0.05$, significant difference compared to matched control. NS — not significant ($P>0.05$) for the comparisons indicated by connected lines. (E) The effects of N7-Smac peptide (15 and 30 μM) on viability of HASM treated with simvastatin (10 μM) for up to 72 h. Cell viability was measured by MTT assay. Data shown are the mean of 12 experiments performed in quadruplicate. *** — $P<0.001$compared to time-matched samples treated with simvastatin alone. (F) The effects of N7-Smac peptide (30 μM) on caspase-9 activation in HASM treated with simvastatin (10 μM) for 36 or 60 h. Caspase-9 activity was measured by Caspase-Glo® luminescence assay. Data shown are the mean of 12 experiments performed in quadruplicate using three different cell lines. *** — $P<0.001$compared to time-matched samples treated with simvastatin alone.

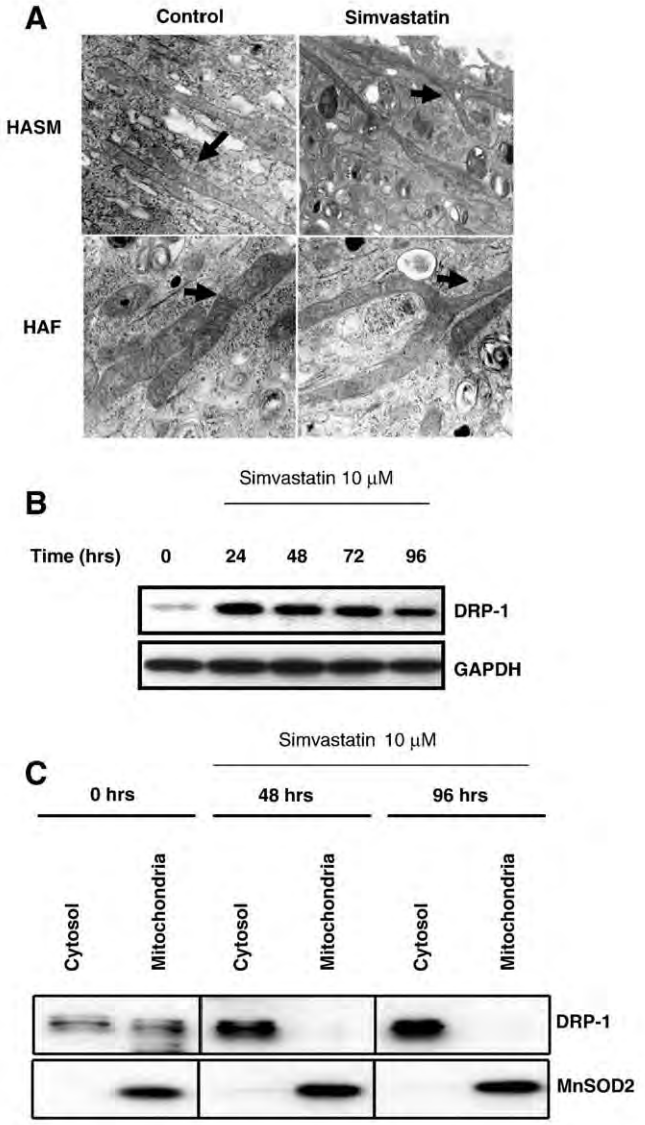

Fig. 7. Simvastatin shows hallmark features of mitochondrial fission inhibition. (A) TEM micrographs of HASM cells (top row) and HAF (bottom row) before (left panel) and after (right panel) simvastatin treatment (10 μM, 72 h). Representative mitochondria are indicated by black arrows. Images are typical of multiple micrographs obtained in at least two different cell cultures. Magnification: HASM = 34×10^3; HAF = 2.65×10^3. (B) Western blot detection of Drp1 (80 kDa) in whole cell lysates of HASM treated with simvastatin (10 μM) for up to 96 h. GAPDH (37 kDa) was used to confirm equal protein loading. Blots shown are typical of those obtained in duplicate from at least three independent cultures. (C) Immunoblots for Drp1 (80 kDa) in cytosol and mitochondrial fractions isolated from HASM treated with simvastatin (10 μM) for 48 or 96 h. Fraction purity and equal sample loading was confirmed by probing for MnSOD2 (21 kDa). Blots shown are typical of those obtained in duplicate from at least three independent cultures.

needed for membrane anchoring of small GTPases including Ras, RhoA, and Rac that have been implicated in death signaling induced by statins [6,8,20]. Our results are consistent with such a mechanism as simvastatin caused a marked loss of membrane-associated Rac1/2/3 and RhoA, and in reconstitution experiments mevalonate, FPP and GGPP all diminished the apoptotic effects of simvastatin, a result that parallels studies with rat vascular smooth muscle cells [5]. In contrast to our findings, depletion of cellular cholesterol has been linked to statin-induced apoptosis in some cancer cells [38], supporting the need for careful dissection of apoptosis mechanisms in healthy cells.

Caspases serve as initiators and executioners of extrinsic and intrinsic apoptotic pathways [10]. In HASM and HAF simvastatin failed to activate caspase-8 or induce Bid cleavage indicating no role for an extrinsic pathway. This contrasts some studies with cancer cells, human umbilical endothelial cells and skeletal myoblasts that show statins can activate caspase-8 [18,19,55], though this is not required for apoptosis in all cell types [18]. This suggests cell-type dependent statin-triggered caspase-8 activation. Our data support a central role for intrinsic apoptosis in primary lung mesenchymal cells, as simvastatin promotes activation of caspase-9 and its downstream executioner cysteine proteases, caspase-7 and -3, as well as cleavage of the distal substrate, PARP-1. This is consistent with studies using cancer cell lines and other primary cell types [18,19,56]. We also uncovered mitochondria-associated mechanisms including increased outer membrane permeability upon statin exposure, which correlates the loss in $\Delta\Psi_m$ in some cancer lines [20]. Notably, we show simvastatin induces intracellular ROS generation, which to our knowledge is a unique observation. The mitochondrial-selective dye we used is sensitive to an oxidation reaction catalyzed by mitochondrial superoxide that can be counteracted by cellular superoxide dismutase. Thus, simvastatin promotes ROS generation via aerobic respiration that overcomes intrinsic antioxidant defenses. This is of functional importance, as we observed that the clinically used antioxidant, NAC, partially suppresses simvastatin-induced HASM and HAF cell death, indicating mitochondrial ROS contribute to the death-triggering effects of statins.

Oxidative stress is a principal signal for genotoxic stress that induces expression and activation of the tumor suppressor gene, p53 [57]. The p53 protein can bind to nearly 300 different promoter elements in the human genome [58], among them *PUMA*, *Bax* and *NOXA* [42], and it broadly alters patterns of gene expression that can support mitochondrial apoptotic pathways [59]. A link between p53 and statin-induced apoptosis has not been clearly established heretofore. Indeed, a previous report using p53 mutant breast cancer cells indicated that lovastatin was able to induce pro-apoptotic mitochondrial mechanisms, including cytochrome *c* release [18]. This contrasts our studies that reveal a central role for p53 in adult HASM cells and HAF; simvastatin activated p53 both by increasing its expression and by fostering phosphorylation of Ser-15 and -37, and this effect was partially required for cell death as the p53-transcriptional inhibitor, cyclic-pifithrin-α [43], significantly reduced mesenchymal cell apoptosis and PARP-1 cleavage. Simvastatin also induced p53-dependent expression of PUMA, NOXA and Bax, as cyclic-pifithrin-α suppressed accumulation of NOXA and PUMA mRNA and protein. Moreover, silencing of the p53-dependent accumulation of PUMA with shRNAi was sufficient to partially prevent apoptosis. These observations underscore an initiator role for p53 in mitochondrial mechanisms as we observed Bax/Bak oligomerization, and marked accumulation of PUMA and NOXA in mitochondria concomitant with the loss of $\Delta\Psi_m$. PUMA and NOXA interact with BH3 domains of cytosol-localized anti-apoptotic proteins such as Bcl-XL that sequester Bax [12,14]. Apoptotic signals can promote Bax translocation to mitochondria [60] and induce allosteric conformational change in mitochondrial Bak [61], thereby inducing formation of mitochondrial permeability pores that reduce $\Delta\Psi_m$ and create a conduit for the release of pro-apoptotic proteins [62,63]. This mechanism is initiated by p53 in simvastatin-treated adult lung mesenchymal cells, however, our data suggest that it is not sufficient to account fully for the apoptotic response, and unlike cancer cells [18] cytochrome *c* release does not appear to be involved.

Several molecules are released from the mitochondrial inter-membrane space in response to apoptotic stimuli. Some well-characterized proteins include cytochrome *c*, Smac, Omi, AIF and Endo G [64]. The release of cytochrome *c*, Smac and Omi leads to the proteolytic (auto) activation of caspase-9, which is further sustained by positive feedback involving activated caspase-3 [10]. We observed Bax/Bak oligomerization, Bax, PUMA, and NOXA mitochondrial translocation, and the release of Smac and Omi but not cytochrome *c*, AIF or Endo G from mitochondria

upon simvastatin treatment. Smac, Omi and cytochrome *c* are more-or-less soluble in the inter-membrane space whereas AIF is anchored in the inner membrane space [65] and Endo G is localized in the matrix [66], perhaps explaining why the latter are not released by simvastatin exposure. As cytochrome *c*, Smac and Omi release is typically a concomitant event with similar kinetic profiles [28,67,68], our observations indicating the uncoupling of this relationship are unique and provocative. Moreover, we and others have reported that the inhibition of mitochondrial fission promotes release of Smac, but not cytochrome *c*, and leads to Bax/Bak-dependent apoptosis [16,47,48]. We confirmed this observation in HASM and HAF with independent experiments that also assessed the functional relevance of our findings; simvastatin-induced caspase-9 activation and apoptosis was refractory to the apoptosome-selective inhibitor, NS3694, thus confirming no significant role for mitochondrial cytochrome *c* release. These findings suggest cytochrome *c*, a component of mitochondrial respiratory chain, may be loosely attached to the inner mitochondrial membrane via protein–protein interactions, making it less prone to release than Smac and Omi under some conditions. Of particular interest are reports that indicate Smac and Omi are more loosely bound to the mitochondria than cytochrome *c* in Drp1-depleted mitochondria [69]. Indeed, differential release of cytochrome *c*, Smac, Omi and other inter-membrane proteins has been observed during Bax/Bak-dependent apoptosis in Drp1-deficient cells [16,47]. These observations correlate well with our data showing almost all mitochondrial Drp1 was lost whilst cytosolic levels increased markedly upon simvastatin exposure. Drp1 is a large GTPase that associates with mitochondria where it couples GTP hydrolysis with mitochondrial membrane constriction and fission [70]. Of note, we observed that simvastatin promoted formation of large forkhead mitochondria that are a hallmark of suppressed mitochondrial fission, strongly suggesting simvastatin disrupted mitochondrial dynamics concomitant with the loss of Drp1 from the organelles. Interestingly, Drp1 is a GTPase and its translocation from mitochondrial membrane to cytosol might be explained by simvastatin inhibition of protein prenylation, however this mechanism needs to be clarified.

The mitochondrial pro-apoptotic protein Smac interferes with IAP-mediated caspase inhibition in several cell death models [48,71]. Thus, Smac released during simvastatin treatment could promote cell death by relieving IAP inhibition of caspase-9, -3 and -7 [72]. In our experimental system Smac N7 peptide further compromised cell viability supporting the concept that increased release of Smac can promote simvastatin-induced apoptosis in adult human airway mesenchymal cells. Smac N7 does not contain the Smac dimerization domain needed to inhibit XIAP but it does contain an IBM domain that binds the XIAP initiator caspase binding site, therefore the peptide directly mitigates mechanisms that suppress caspase-9 (auto)activation [73]. Overall, our observations provide support for a simvastatin-induced pro-apoptotic pathway that relies on activation of caspases-9, -7 and -3 by Smac, which is released from mitochondria due both to Bax/Bak-dependent mitochondrial permeability driven by p53-PUMA, and the disruption of mitochondrial fission resulting from a loss of mitochondrial Drp1. Our data also suggest that this pathway may be linked to reduced prenylation of signaling proteins, thus our group is currently focused on identifying the pathways that might play a role in simvastatin-induced cell death in human airway mesenchymal cells.

Acknowledgements

The authors would like to thank Ms. Karen A. Detillieux for her editorial contribution to this manuscript. This work was supported by grants from the Canadian Institutes of Health Research (CIHR), GlaxoSmithKline Collaborative Innovation Research Fund, Manitoba Institute of Child Health, and Canada Foundation for Innovation. SG is supported by a CIHR/Canadian Lung Association/GlaxoSmithKline Postdoctoral fellowship, and a personnel award from the National Training Program in Allergy and Asthma (NTPAA). KH was supported by a Manitoba Health research Council (MHRC) studentship. DS is supported by a MHRC/Manitoba Institute of Child Health (MICH) Postdoctoral Fellowship, and holds a CIHR IMPACT Strategic Training Postdoctoral fellowship. PS and TH are supported by personnel awards from the NTPAA, MHRC and MICH. PS is supported by a University of Manitoba Graduate Fellowship. SKK is a Basic Science Career Development Research Awardee of the Manitoba Medical Service Foundation supported with funds provided by the Manitoba Blue Cross, and the Biomedical Functionality Resource he directs was established under the support of Dean Strategic Research Fund, Faculty of Medicine at University of Manitoba. GMH is a Canada Research Chair in Molecular Cardiolipin Metabolism. TK acknowledges the support by the Natural Sciences and Engineering Research Council of Canada (NSERC). ML thankfully acknowledges the support from DFG (SFB 773, GRK 1302) and Deutsche Krebshilfe. AJH holds a Canada Research Chair in Airway Cell and Molecular Biology.

References

[1] J.L. Goldstein, M.S. Brown, Regulation of the mevalonate pathway, Nature 343 (1990) 425–430.
[2] J.K. Liao, U. Laufs, Pleiotropic effects of statins, Annu. Rev. Pharmacol. Toxicol. 45 (2005) 89–118.
[3] M.F. Demierre, P.D. Higgins, S.B. Gruber, E. Hawk, S.M. Lippman, Statins and cancer prevention, Nat. Rev. Cancer 5 (2005) 930–942.
[4] W.W. Wong, J. Dimitroulakos, M.D. Minden, L.Z. Penn, HMG-CoA reductase inhibitors and the malignant cell: the statin family of drugs as triggers of tumor-specific apoptosis, Leukemia 16 (2002) 508–519.
[5] C. Guijarro, L.M. Blanco-Colio, M. Ortego, C. Alonso, A. Ortiz, J.J. Plaza, C. Diaz, G. Hernandez, J. Egido, 3-Hydroxy-3-methylglutaryl coenzyme a reductase and isoprenylation inhibitors induce apoptosis of vascular smooth muscle cells in culture, Circ. Res. 83 (1998) 490–500.
[6] J. Heusinger-Ribeiro, B. Fischer, M. Goppelt-Struebe, Differential effects of simvastatin on mesangial cells, Kidney Int. 66 (2004) 187–195.
[7] K. Yokota, F. Miyoshi, T. Miyazaki, K. Sato, Y. Yoshida, Y. Asanuma, Y. Akiyama, T. Mimura, High concentration simvastatin induces apoptosis in fibroblast-like synoviocytes from patients with rheumatoid arthritis, J. Rheumatol. 35 (2008) 193–200.
[8] J. Wu, W.W. Wong, F. Khosravi, M.D. Minden, L.Z. Penn, Blocking the Raf/MEK/ERK pathway sensitizes acute myelogenous leukemia cells to lovastatin-induced apoptosis, Cancer Res. 64 (2004) 6461–6468.
[9] J.K. Liao, Isoprenoids as mediators of the biological effects of statins, J. Clin. Invest. 110 (2002) 285–288.
[10] S. Ghavami, M. Hashemi, S.R. Ande, B. Yeganeh, W. Xiao, M. Eshraghi, C.J. Bus, K. Kadkhoda, E. Wiechec, A.J. Halayko, M. Los, Apoptosis and cancer: mutations within caspase genes, J. Med. Genet. 46 (2009) 497–510.
[11] S. Cory, J.M. Adams, The Bcl2 family: regulators of the cellular life-or-death switch, Nat. Rev. Cancer 2 (2002) 647–656.
[12] S.N. Willis, L. Chen, G. Dewson, A. Wei, E. Naik, J.I. Fletcher, J.M. Adams, D.C. Huang, Proapoptotic Bak is sequestered by Mcl-1 and Bcl-xL, but not Bcl-2, until displaced by BH3-only proteins, Genes Dev. 19 (2005) 1294–1305.
[13] J.E. Chipuk, L. Bouchier-Hayes, T. Kuwana, D.D. Newmeyer, D.R. Green, PUMA couples the nuclear and cytoplasmic proapoptotic function of p53, Science 309 (2005) 1732–1735.
[14] W.X. Zong, T. Lindsten, A.J. Ross, G.R. MacGregor, C.B. Thompson, BH3-only proteins that bind pro-survival Bcl-2 family members fail to induce apoptosis in the absence of Bax and Bak, Genes Dev. 15 (2001) 1481–1486.
[15] N.A. Thornberry, Y. Lazebnik, Caspases: enemies within, Science 281 (1998) 1312–1316.
[16] S. Ghavami, C. Kerkhoff, W.J. Chazin, K. Kadkhoda, W. Xiao, A. Zuse, M. Hashemi, M. Eshraghi, K. Schulze-Osthoff, T. Klonisch, M. Los, S100A8/9 induces cell death via a novel, RAGE-independent pathway that involves selective release of Smac/DIABLO and Omi/HtrA2, Biochim. Biophys. Acta 1783 (2008) 297–311.
[17] H. Zou, Y. Li, X. Liu, X. Wang, An APAF-1.cytochrome *c* multimeric complex is a functional apoptosome that activates procaspase-9, J. Biol. Chem. 274 (1999) 11549–11556.
[18] M.A. Shibata, Y. Ito, J. Morimoto, Y. Otsuki, Lovastatin inhibits tumor growth and lung metastasis in mouse mammary carcinoma model: a p53-independent mitochondrial-mediated apoptotic mechanism, Carcinogenesis 25 (2004) 1887–1898.
[19] M. Marcelli, G.R. Cunningham, S.J. Haidacher, S.J. Padayatty, L. Sturgis, C. Kagan, L. Denner, Caspase-7 is activated during lovastatin-induced apoptosis of the prostate cancer cell line LNCaP, Cancer Res. 58 (1998) 76–83.
[20] P. Cafforio, F. Dammacco, A. Gernone, F. Silvestris, Statins activate the mitochondrial pathway of apoptosis in human lymphoblasts and myeloma cells, Carcinogenesis 26 (2005) 883–891.
[21] J.A. Elias, Z. Zhu, G. Chupp, R.J. Homer, Airway remodeling in asthma, J. Clin. Invest. 104 (1999) 1001–1006.
[22] N. Regamey, M. Ochs, T.N. Hilliard, C. Muhlfeld, N. Cornish, L. Fleming, S. Saglani, E. W. Alton, A. Bush, P.K. Jeffery, J.C. Davies, Increased airway smooth muscle mass in children with asthma, cystic fibrosis, and non-cystic fibrosis bronchiectasis, Am. J. Respir. Crit. Care Med. 177 (2008) 837–843.

[23] E. Hothersall, C. McSharry, N.C. Thomson, Potential therapeutic role for statins in respiratory disease, Thorax 61 (2006) 729–734.
[24] F. Ratjen, New pulmonary therapies for cystic fibrosis, Curr. Opin. Pulm. Med. 13 (2007) 541–546.
[25] A.A. Zeki, L. Franzi, J. Last, N.J. Kenyon, Simvastatin inhibits airway hyperreactivity: implications for the mevalonate pathway and beyond, Am. J. Respir. Crit. Care Med. 180 (2009) 731–740.
[26] R. Gosens, G.L. Stelmack, G. Dueck, K.D. McNeill, A. Yamasaki, W.T. Gerthoffer, H. Unruh, A.S. Gounni, J. Zaagsma, A.J. Halayko, Role of caveolin-1 in p42/p44 MAP kinase activation and proliferation of human airway smooth muscle, Am. J. Physiol. Lung Cell. Mol. Physiol. 291 (2006) L523–L534.
[27] E.T. Naureckas, I.M. Ndukwu, A.J. Halayko, C. Maxwell, M.B. Hershenson, J. Solway, Bronchoalveolar lavage fluid from asthmatic subjects is mitogenic for human airway smooth muscle, Am. J. Respir. Crit. Care Med. 160 (1999) 2062–2066.
[28] S. Ghavami, M. Eshraghi, K. Kadkhoda, M.M. Mutawe, S. Maddika, G.H. Bay, S. Wesselborg, A.J. Halayko, T. Klonisch, M. Los, Role of BNIP3 in TNF-induced cell death—TNF upregulates BNIP3 expression, Biochim. Biophys. Acta 1793 (2009) 546–560.
[29] S. Ghavami, A. Asoodeh, T. Klonisch, A. Halayko, K. Kadkhoda, K.T., S.B. Gibson, E.P. Booy, H. Naderi-Manesh, M. Los, Brevinin-2R semi-selectively kills cancer cells by a distinct mechanism, which involves the lysosomal-mitochondrial death pathway, J. Cell. Mol. Med. (2008) 1–18.
[30] M. Zhou, Z. Diwu, N. Panchuk-Voloshina, R.P. Haugland, A stable nonfluorescent derivative of resorufin for the fluorometric determination of trace hydrogen peroxide: applications in detecting the activity of phagocyte NADPH oxidase and other oxidases, Anal. Biochem. 253 (1997) 162–168.
[31] J.G. Mohanty, J.S. Jaffe, E.S. Schulman, D.G. Raible, A highly sensitive fluorescent micro-assay of H2O2 release from activated human leukocytes using a dihydroxyphenoxazine derivative, J. Immunol. Methods 202 (1997) 133–141.
[32] V. Mokashi, D.K. Singh, T.D. Porter, Supernatant protein factor stimulates HMG-CoA reductase in cell culture and in vitro, Arch. Biochem. Biophys. 433 (2005) 474–480.
[33] D. Tang, H.J. Park, S.P. Georgescu, S.M. Sebti, A.D. Hamilton, J.B. Galper, Simvastatin potentiates tumor necrosis factor alpha-mediated apoptosis of human vascular endothelial cells via the inhibition of the geranylgeranylation of RhoA, Life Sci. 79 (2006) 1484–1492.
[34] C. Adrain, E.M. Creagh, S.J. Martin, Apoptosis-associated release of Smac/DIABLO from mitochondria requires active caspases and is blocked by Bcl-2, EMBO J. 20 (2001) 6627–6636.
[35] J. Tran, S.K. Kung, Lentiviral vectors mediate stable and efficient gene delivery into primary murine natural killer cells, Mol. Ther. 15 (2007) 1331–1339.
[36] P. Sharma, T. Tran, G.L. Stelmack, K. McNeill, R. Gosens, M.M. Mutawe, H. Unruh, W.T. Gerthoffer, A.J. Halayko, Expression of the dystrophin–glycoprotein complex is a marker for human airway smooth muscle phenotype maturation, Am. J. Physiol. Lung Cell. Mol. Physiol. 294 (2008) L57–L68.
[37] N.W. van de Donk, M.M. Kamphuis, B. van Kessel, H.M. Lokhorst, A.C. Bloem, Inhibition of protein geranylgeranylation induces apoptosis in myeloma plasma cells by reducing Mcl-1 protein levels, Blood 102 (2003) 3354–3362.
[38] L. Zhuang, J. Kim, R.M. Adam, K.R. Solomon, M.R. Freeman, Cholesterol targeting alters lipid raft composition and cell survival in prostate cancer cells and xenografts, J. Clin. Invest. 115 (2005) 959–968.
[39] R. Gniadecki, Depletion of membrane cholesterol causes ligand-independent activation of Fas and apoptosis, Biochem. Biophys. Res. Commun. 320 (2004) 165–169.
[40] J.E. Chipuk, T. Kuwana, L. Bouchier-Hayes, N.M. Droin, D.D. Newmeyer, M. Schuler, D.R. Green, Direct activation of Bax by p53 mediates mitochondrial membrane permeabilization and apoptosis, Science 303 (2004) 1010–1014.
[41] S. Maddika, S.R. Ande, S. Panigrahi, T. Paranjothy, K. Weglarczyk, A. Zuse, M. Eshraghi, K.D. Manda, E. Wiechec, M. Los, Cell survival, cell death and cell cycle pathways are interconnected: implications for cancer therapy, Drug Resist. Updat. 10 (2007) 13–29.
[42] K.H. Vousden, X. Lu, Live or let die: the cell's response to p53, Nat. Rev. Cancer 2 (2002) 594–604.
[43] P.G. Komarov, E.A. Komarova, R.V. Kondratov, K. Christov-Tselkov, J.S. Coon, M.V. Chernov, A.V. Gudkov, A chemical inhibitor of p53 that protects mice from the side effects of cancer therapy, Science 285 (1999) 1733–1737.
[44] Z. Abdullaev, M.E. Bodrova, B.V. Chernyak, D.A. Dolgikh, R.M. Kluck, M.O. Pereverzev, A.S. Arseniev, R.G. Efremov, M.P. Kirpichnikov, E.N. Mokhova, D.D. Newmeyer, H. Roder, V.P. Skulachev, A cytochrome *c* mutant with high electron transfer and antioxidant activities but devoid of apoptogenic effect, Biochem J. 362 (2002) 749–754.
[45] V. Bilim, K. Yuuki, T. Itoi, A. Muto, T. Kato, A. Nagaoka, T. Motoyama, Y. Tomita, Double inhibition of XIAP and Bcl-2 axis is beneficial for retrieving sensitivity of renal cell cancer to apoptosis, Br. J. Cancer 98 (2008) 941–949.
[46] A. Tanaka, R.J. Youle, A chemical inhibitor of DRP1 uncouples mitochondrial fission and apoptosis, Mol. Cell 29 (2008) 409–410.
[47] P.A. Parone, J.C. Martinou, Mitochondrial fission and apoptosis: an ongoing trial, Biochim. Biophys. Acta 1763 (2006) 522–530.
[48] P.A. Parone, D.I. James, S. Da Cruz, Y. Mattenberger, O. Donze, F. Barja, J.C. Martinou, Inhibiting the mitochondrial fission machinery does not prevent Bax/Bak-dependent apoptosis, Mol. Cell. Biol. 26 (2006) 7397–7408.
[49] D.I. James, P.A. Parone, Y. Mattenberger, J.C. Martinou, hFis1, a novel component of the mammalian mitochondrial fission machinery, J. Biol. Chem. 278 (2003) 36373–36379.
[50] C.J. Vaughan, M.B. Murphy, B.M. Buckley, Statins do more than just lower cholesterol, Lancet 348 (1996) 1079–1082.
[51] S. Demyanets, C. Kaun, S. Pfaffenberger, P.J. Hohensinner, G. Rega, J. Pammer, G. Maurer, K. Huber, J. Wojta, Hydroxymethylglutaryl-coenzyme A reductase inhibitors induce apoptosis in human cardiac myocytes in vitro, Biochem. Pharmacol. 71 (2006) 1324–1330.
[52] A.M. Connor, S. Berger, A. Narendran, E.C. Keystone, Inhibition of protein geranylgeranylation induces apoptosis in synovial fibroblasts, Arthritis Res. Ther. 8 (2006) R94.
[53] P. Negre-Aminou, A.K. van Vliet, M. van Erck, G.C. van Thiel, R.E. van Leeuwen, L.H. Cohen, Inhibition of proliferation of human smooth muscle cells by various HMG-CoA reductase inhibitors; comparison with other human cell types, Biochim. Biophys. Acta 1345 (1997) 259–268.
[54] O. Stein, J. Vanderhoek, G. Friedman, Y. Stein, Deposition and mobilization of cholesterol ester in cultured human skin fibroblasts, Biochim. Biophys. Acta 450 (1976) 367–378.
[55] M. Diamant, M.E. Tushuizen, M.N. Abid-Hussein, C.M. Hau, A.N. Boing, A. Sturk, R. Nieuwland, Simvastatin-induced endothelial cell detachment and microparticle release are prenylation dependent, Thromb. Haemost. 100 (2008) 489–497.
[56] L.M. Blanco-Colio, A. Villa, M. Ortego, M.A. Hernandez-Presa, A. Pascual, J.J. Plaza, J. Egido, 3-Hydroxy-3-methyl-glutaryl coenzyme A reductase inhibitors, atorvastatin and simvastatin, induce apoptosis of vascular smooth muscle cells by downregulation of Bcl-2 expression and Rho A prenylation, Atherosclerosis 161 (2002) 17–26.
[57] J.L. Martindale, N.J. Holbrook, Cellular response to oxidative stress: signaling for suicide and survival, J. Cell. Physiol. 192 (2002) 1–15.
[58] C.L. Wei, Q. Wu, V.B. Vega, K.P. Chiu, P. Ng, T. Zhang, A. Shahab, H.C. Yong, Y. Fu, Z. Weng, J. Liu, X.D. Zhao, J.L. Chew, Y.L. Lee, V.A. Kuznetsov, W.K. Sung, L.D. Miller, B. Lim, E.T. Liu, Q. Yu, H.H. Ng, Y. Ruan, A global map of p53 transcription-factor binding sites in the human genome, Cell 124 (2006) 207–219.
[59] M. Schuler, U. Maurer, J.C. Goldstein, F. Breitenbucher, S. Hoffarth, N.J. Waterhouse, D.R. Green, p53 triggers apoptosis in oncogene-expressing fibroblasts by the induction of Noxa and mitochondrial Bax translocation, Cell Death Differ. 10 (2003) 451–460.
[60] T. Mashima, T. Tsuruo, Defects of the apoptotic pathway as therapeutic target against cancer, Drug Resist. Updat. 8 (2005) 339–343.
[61] A. Gross, J.M. McDonnell, S.J. Korsmeyer, BCL-2 family members and the mitochondria in apoptosis, Genes Dev. 13 (1999) 1899–1911.
[62] J. Yu, L. Zhang, P.M. Hwang, K.W. Kinzler, B. Vogelstein, PUMA induces the rapid apoptosis of colorectal cancer cells, Mol. Cell 7 (2001) 673–682.
[63] T. Shibue, K. Takeda, E. Oda, H. Tanaka, H. Murasawa, A. Takaoka, Y. Morishita, S. Akira, T. Taniguchi, N. Tanaka, Integral role of Noxa in p53-mediated apoptotic response, Genes Dev. 17 (2003) 2233–2238.
[64] S.J. Riedl, Y. Shi, Molecular mechanisms of caspase regulation during apoptosis, Nat. Rev. Mol. Cell. Biol. 5 (2004) 897–907.
[65] H. Otera, S. Ohsakaya, Z. Nagaura, N. Ishihara, K. Mihara, Export of mitochondrial AIF in response to proapoptotic stimuli depends on processing at the intermembrane space, EMBO J. 24 (2005) 1375–1386.
[66] D. Arnoult, B. Gaume, M. Karbowski, J.C. Sharpe, F. Cecconi, R.J. Youle, Mitochondrial release of AIF and EndoG requires caspase activation downstream of Bax/Bak-mediated permeabilization, EMBO J. 22 (2003) 4385–4399.
[67] G. van Loo, M. van Gurp, B. Depuydt, S.M. Srinivasula, I. Rodriguez, E.S. Alnemri, K. Gevaert, J. Vandekerckhove, W. Declercq, P. Vandenabeele, The serine protease Omi/HtrA2 is released from mitochondria during apoptosis. Omi interacts with caspase-inhibitor XIAP and induces enhanced caspase activity, Cell Death Differ. 9 (2002) 20–26.
[68] T.M. Bocan, Pleiotropic effects of HMG-CoA reductase inhibitors, Curr. Opin. Investig. Drugs 3 (2002) 1312–1317.
[69] A. Laurent, C. Nicco, C. Chereau, C. Goulvestre, J. Alexandre, A. Alves, E. Levy, F. Goldwasser, Y. Panis, O. Soubrane, B. Weill, F. Batteux, Controlling tumor growth by modulating endogenous production of reactive oxygen species, Cancer Res. 65 (2005) 948–956.
[70] E. Smirnova, D.L. Shurland, S.N. Ryazantsev, A.M. van der Bliek, A human dynamin-related protein controls the distribution of mitochondria, J. Cell. Biol. 143 (1998) 351–358.
[71] N. Ishihara, M. Nomura, A. Jofuku, H. Kato, S.O. Suzuki, K. Masuda, H. Otera, Y. Nakanishi, I. Nonaka, Y. Goto, N. Taguchi, H. Morinaga, M. Maeda, R. Takayanagi, S. Yokota, K. Mihara, Mitochondrial fission factor Drp1 is essential for embryonic development and synapse formation in mice, Nat. Cell. Biol. 11 (2009) 958–966.
[72] P. Maycotte, S. Blancas, J. Moran, Role of inhibitor of apoptosis proteins and Smac/DIABLO in staurosporine-induced cerebellar granule neurons death, Neurochem. Res. 33 (2008) 1534–1540.
[73] S.M. Srinivasula, R. Hegde, A. Saleh, P. Datta, E. Shiozaki, J. Chai, R.A. Lee, P.D. Robbins, T. Fernandes-Alnemri, Y. Shi, E.S. Alnemri, A conserved XIAP-interaction motif in caspase-9 and Smac/DIABLO regulates caspase activity and apoptosis, Nature 410 (2001) 112–116.